

1 **Enhanced Sulfate Formation in Mixed Biomass Burning and Sea-salt**  
2 **Interactions Mediated by Photosensitization: Effects of Chloride,**  
3 **Nitrogen-containing Compounds, and Atmospheric Aging**

4 Rongzhi Tang<sup>1,2</sup>, Jialiang Ma<sup>3</sup>, Ruifeng Zhang<sup>4</sup>, Weizhen Cui<sup>1</sup>, Yuanyuan Qin<sup>5</sup>, Yangxi Chu<sup>6</sup>,  
5 Yiming Qin<sup>1</sup>, Alexander L. Vogel<sup>3</sup>, Chak K. Chan<sup>4,\*</sup>

6 <sup>1</sup> School of Energy and Environment, City University of Hong Kong, Hong Kong, China

7 <sup>2</sup> Shenzhen Research Institute, City University of Hong Kong, Shenzhen 518057, China

8 <sup>3</sup> Institute for Atmospheric and Environmental Sciences, Goethe-University Frankfurt, 60438  
9 Frankfurt am Main, Germany

10 <sup>4</sup> Division of Physical Science and Engineering, King Abdullah University of Science and  
11 Technology (KAUST), Thuwal 23955-6900, Kingdom of Saudi Arabia

12 <sup>5</sup> College of Resources and Environment, University of Chinese Academy of Sciences, Beijing,  
13 100049, China

14 <sup>6</sup> State Key Laboratory of Environmental Criteria and Risk Assessment, Chinese Research  
15 Academy of Environmental Sciences, Beijing, 100012, China

16 *Correspondence to:* Chak K. Chan (chak.chan@kaust.edu.sa)

17 **Abstract**

18 Discrepancies persist between modeled simulations and measured sulfate concentrations in the  
19 marine boundary layer, especially when the marine air is influenced by biomass burning plumes.  
20 However, there is a notable dearth of research conducted on the interactions between sea-salt  
21 aerosol and biomass burning plumes, impeding a comprehensive understanding of the sulfate  
22 formation. This work studied sulfate formation by mixing real biomass burning (BB) extracts  
23 and NaCl, mimicking internal mixtures of BB and sea-salt particles. BB-NaCl particles had  
24 significantly higher sulfate formation rate than incense burning (IS)-NaCl particles. For fresh  
25 particles, the sulfate formation rate followed the trend of corn straw (CS)-NaCl>rice straw  
26 (RS)-NaCl>wheat straw (WS)-NaCl>IS-NaCl. The filter sample aging was achieved by  
27 exposure to OH• generated from UV irradiation. After aging, RS-NaCl particles exhibited the  
28 highest enhancement in sulfate formation rates among all the BB-NaCl particles, due to  
29 interactions between RS and NaCl. Bulk aqueous experiments spiked with NaCl using mixtures  
30 of model photosensitizers (PS) and nitrogen-containing organic compounds (NOCs), pyrazine  
31 (CHN) and 4-nitrocatechol (CHON), revealed positive effects of chloride in the PS-CHON  
32 system and negative effects in the PS-CHN system in sulfate formation. Our work suggests that  
33 BB reaching or near coastal areas can affect sulfate formation via photosensitizer-mediated  
34 reactions, potentially exacerbating air pollution.

35 **Keywords:** sulfate formation, biomass burning, photosensitization, sea-salt aerosol, chloride

## 36 **1 Introduction**

37 Recent fire outbreaks in areas like Canada, Amazonia, and Southeast Australia, together with  
38 the increased fire frequency and intensity reports in areas like western US have highlighted the  
39 risks of fire, especially biomass burning (BB), to human health and climate change (Bond et  
40 al., 2013; Andreae, 2019; Jones et al., 2022). As an agricultural powerhouse, China boasts  
41 immense agricultural crop yields, especially in rice, wheat, and corn throughout the country.  
42 These crop residues are frequently burned in rural areas for cooking and heating purposes, as  
43 well as for land preparation after harvest, resulting in the substantial production of light-  
44 absorbing species, such as brown carbon (BrC) (Chen et al., 2017). Recent studies have reported  
45 that specific BrC species from biomass burning, including vanillin (VL), acetovanillone,  
46 syringaldehyde (SyrAld), and naphthalene-derived secondary organic aerosol (Teich et al.,  
47 2016; Li et al., 2024; Liu et al., 2020; Wang et al., 2021b) can act as photosensitizers (PS) and  
48 oxidize SO<sub>2</sub> to sulfate (Zhou et al., 2023; Liang et al., 2024). Atmospheric processes like aging  
49 or long-range transport, can alter the chemical compositions and optical properties of PS, and  
50 hence affect the sulfate formation potential (You et al., 2020; Li et al., 2019). Sea-salt aerosol  
51 (SSA), with its high particulate matter loadings and extensive surface area, plays a significant  
52 role in interfacial and multiphase reactions with reactive gases, thereby impacting global  
53 radiation balance and air quality in marine and coastal areas (Gantt and Meskhidze, 2013; Chi  
54 et al., 2015). Prior research has identified several secondary sulfate formation pathways in SSA,  
55 e.g., multiphase SO<sub>2</sub> oxidation by O<sub>3</sub> (Alexander et al., 2012), coexistence of NO<sub>2</sub> (Zhang and  
56 Chan, 2023b), PS (Tang et al., 2023), chlorine-PS synergistic effects (Zhang and Chan, 2024),  
57 and Cl and OH radicals generated by chlorine photoactivation (Cao et al., 2024). The  
58 chlorine/chloride studies are particularly interesting as they highlight the importance of NaCl-  
59 based photochemistry in sulfate formation.

60 SSA can frequently mix with organic matter through processes such as sea-to-air emission,  
61 photochemical oxidation and atmospheric transport (Liu et al., 2023b). Previous studies have  
62 observed elevated sulfate concentrations in coastal regions when air masses passed through  
63 inland areas due to intensive BB or other anthropogenic emissions, suggesting the possible  
64 interactions between the SSA (primarily sodium chloride) and anthropogenic emissions (Qiu et  
65 al., 2019; Huang et al., 2018; Wu et al., 2022). Van Pinxteren et al. (2015) observed an increase  
66 in sulfate concentration (2.26 μg m<sup>-3</sup>) during the RV MARIA S cruise as it approached the  
67 African mainland, in contrast to the marine-origin aerosol (1.59 μg m<sup>-3</sup>), showing significant  
68 influence of BB. Hence, mixing of sea-salt and biomass burning aerosols can lead to secondary  
69 aerosol production in coastal regions.

70 Transmission electron microscopy (TEM) studies indicate that most coastal particles are  
71 internally mixed, showing a higher proportion of organic and salt mixtures in the presence of  
72 biomass burning aerosols, accompanied by an increase in sulfate (Dang et al., 2022; Li et al.,  
73 2003). However, discrepancies persist between modeled simulations and measured sulfate  
74 concentrations in MBL (Yu et al., 2023). The interactions of sea-salt and BB aerosols, especially  
75 in multiphase reactions, can potentially unravel the intricate chemistry of sulfate formation in  
76 BB affected MBL. Hence, internal mixtures of inorganic salt and water-soluble organic carbons

77 are often used in reaction studies (Tan et al., 2024).

78 The two main atmospheric water systems in marine boundary layer (MBL) were wet aerosol  
79 (droplets in our case) and cloud/fog (bulk aqueous solutions), both droplet and aqueous  
80 reactions are relevant for studying multiphase sulfate formation within MBL (Ruiz-Lopez et al.,  
81 2020; Herrmann, 2003). Typically, droplet reactions were characterized by high ionic strength  
82 (up to >10 M), low liquid water content ( $10^{-7}$ - $10^{-3}$  cm<sup>3</sup> m<sup>-3</sup>) and high surface-to-volume ratio  
83 whereas aqueous reactions exhibit the opposite characteristics. Additionally, droplet  
84 experiments can encompass certain interfacial reaction pathways that may occur in the  
85 atmosphere, especially in submicron particles (Ruiz-Lopez et al., 2020).

86 Previous studies have detected a significant proportion of NOCs, including nitroaromatics  
87 (CHON) and reduced nitrogen species (CHN) in biomass burning plumes, wildfires and  
88 ambient samples (Zhong et al., 2024; Wang et al., 2017b; Song et al., 2022; Cai et al., 2020).  
89 These NOCs are considered ubiquitous contributors to BrC and can affect global climate and  
90 human health. Moreover, recent research has discovered aerosol pollution in marine  
91 background regions, with high levels of NOCs when air masses are transported from wildfires  
92 or biomass burning events in nearby (Zhong et al., 2024; Qin et al., 2024). These NOCs,  
93 combined with reactive gases, may mix with SSA and impact regional air quality in coastal  
94 zones. Therefore, it is essential to further investigate the interactions between NOCs, reactive  
95 gases, and SSA.

96 In this study, we performed in-situ droplet and bulk aqueous solution reaction experiments  
97 using BB extracts-NaCl mixtures to explore the possible interplay between biomass burning  
98 and marine aerosols in coastal areas. BB was derived from the burning of rice straw (RS), wheat  
99 straw (WS), and corn straw (CS) as well as incense burning (IS). The aims of this study are to:  
100 (i) compare the differences in sulfate formation among different kinds of BB-NaCl particles  
101 and BB extracts; (ii) examine the impacts of OH• aging on sulfate formation across different  
102 BB-NaCl particles and BB extracts; (iii) investigate the role of NOCs and chloride ions in BB  
103 extracts mediated sulfate formation.

## 104 **2 Material and methods**

### 105 **2.1 Burning experiments**

106 Three types of commonly used biomass (RS, WS and CS) were cut into small, uniform pieces  
107 (~10 cm in length) and dried. About 100 g of the dried biomass materials (~10% moisture  
108 content) was then introduced into a traditional iron stove commonly used in rural areas (Figure  
109 S1). The stove was covered with a hood and the biomass was ignited using a propane lighter.  
110 The generated BB smoke was collected onto 90-mm quartz filters at  $0.9 \text{ m}^3 \text{ min}^{-1}$  for 10 minutes  
111 by a custom-made aerosol sampler under mixed combustion conditions (include flaming and  
112 smoldering, modified combustion efficiency MCE,  $0.85 \leq \Delta[\text{CO}_2]/(\Delta[\text{CO}_2]+\Delta[\text{CO}]) \leq 0.95$ )  
113 (Ting et al., 2018). The sampler was placed 1 meter above the ground and connected to a PM<sub>2.5</sub>  
114 sampling head through a sampling pump. For incense burning (IS), laboratory-generated  
115 smoldering smoke was collected on 47-mm quartz filters at a flow rate of ~  $6.0 \text{ L min}^{-1}$  for 80  
116 min using a stainless-steel combustion chamber. Note that the different combustion modes of

117 IS and BB are intentionally used to represent real-world combustion conditions. Our previous  
118 study demonstrated that IS was representative of BB based on GC×GC chromatograms and  
119 pixel-based partial least squares discriminant analysis (Tang et al., 2023). Hereafter, we will  
120 use BB to represent both the real BB materials and the surrogate materials (IS) unless otherwise  
121 specified. After sampling, the collected BB samples (fresh BB) were wrapped by pre-baked  
122 aluminum foil (550 °C for 6 h) and stored at -20 °C until further analysis.

123 To achieve atmospheric OH• aging, the collected fresh BB filter samples were placed in a pre-  
124 flushed chamber (zero air, more than 24 h) and illuminated with UV lamps for 40 min. We used  
125 lamps of 185 nm and 254 nm, the combination of which has been widely used in oxidation flow  
126 reactor design and experiments for mimicking atmospheric OH• aging conditions (Peng and  
127 Jimenez, 2020; Rowe et al., 2020; Tkacik et al., 2014; Hu et al., 2022). The estimated OH  
128 exposure was  $\sim 2.0 \times 10^{12}$  molecules  $\text{cm}^{-3}$  s, equivalent to an atmospheric aging period of 15  
129 days (assuming an average atmospheric OH concentration of  $1.5 \times 10^6$  molecules  $\text{cm}^{-3}$ ) (Mao et  
130 al., 2009). Detailed characterization of the OH exposure can be found in our previous study  
131 (Tang et al., 2023). We will discuss the sulfate formation of these fresh and OH• aged samples  
132 later.

## 133 **2.2 Materials and instrumentation**

134 Aqueous stock solutions of BB samples were prepared by dissolving the collected filters in  
135 ultrapure water and subjecting them to ultrasonication in a cooled-water bath three times, each  
136 for 20 minutes. The resulting water extracts of the BB were then filtered through 0.22  $\mu\text{m}$  PTFE  
137 filters and stored in brown vials at 4°C in a refrigerator. The anions, i.e., chloride, sulfate and  
138 nitrate of the BB extracts were analyzed by Dionex ion chromatography (ICS 1100, CA). An  
139 aliquot ( $\sim 0.5$  ml) of the BB or IS extracts was used for water-soluble organics detection by  
140 ultra-high performance liquid chromatography (Thermo Scientific Dionex UltiMate 3000  
141 UHPLC) coupled with high-resolution Orbitrap Fusion Lumos Tribrid mass spectrometry  
142 (Orbitrap HRMS, Thermo Fisher Scientific, USA). The particulate organic matter was  
143 characterized by directly heating the filter samples using a thermal desorption module (TDS3,  
144 Gerstel) coupled to comprehensive two-dimensional gas chromatography-mass spectrometer  
145 (GCMS-TQ™8050 NX, Shimadzu, Japan). UV-Vis spectrometry (UV-3600, Shimadzu, Japan)  
146 was employed to examine the absorbance of BB extracts. Total organic carbon (TOC) was  
147 measured by total carbon analyzer (TOC-L CPH, Shimadzu, Japan). Metal concentrations were  
148 measured by inductively coupled plasma-mass spectrometry (ICP-MS, Agilent 7800). Detailed  
149 analysis can be found in Text S1. Aqueous stock solution of sodium chloride ( $\geq 99.8\%$ , Unichem)  
150 was prepared by dissolving the corresponding salt in ultrapure water to obtain a concentration  
151 of 1M. The study utilized high purity grade synthetic air and nitrogen supplied by the Linde  
152 HKO Ltd., while sulfur dioxide was obtained from the Scientific Gas Engineering Co., Ltd.

## 153 **2.3 Multiphase and aqueous-phase reactions of S(IV)**

154 In SO<sub>2</sub> uptake experiments, the stock solution of BB (fresh and aged) extracts was premixed  
155 with sodium chloride solution (1M) at a volume ratio of 1:1 and the solutions had pH a of 4-6.  
156 A droplet generator (Model 201, Uni-Photon Inc.) was then utilized to deposit droplets onto a  
157 hydrophobic substrate (model 5793, YSI Inc.) for SO<sub>2</sub> uptake experiments. Reactive SO<sub>2</sub> uptake

158 experiments were performed via a flow cell/in-situ Raman system at controlled room  
159 temperature (23-25°C). The top and bottom quartz windows of the flow cell were used for  
160 Raman analysis and UV irradiation, respectively. The light experiment was performed using a  
161 xenon lamp (model 6258, ozone free, 300W, Newport), with photon flux of  $9.8 \times 10^{15}$  photons  
162  $\text{cm}^{-2} \text{s}^{-1}$  in 280-420 nm received by particles in the flow cell (Zhang and Chan, 2023b). Identical  
163 experiments were conducted in the dark, with the lights off and the experimental area kept in  
164 complete darkness. The relative humidity (RH) inside the flow cell was adjusted to 80% by  
165 mixing dry and wet synthetic air or nitrogen. The particles were then equilibrated at 80% RH  
166 for over 60 min and remained liquid throughout the experiment period.  $\text{SO}_2$  was introduced  
167 into the system to reach a concentration of 8.0 ppm. The prescribed size used in our in-situ  
168 Raman research was  $60 \pm 5 \mu\text{m}$ . Despite using particles for droplet experiments that were larger  
169 than ambient fine particles, we employed the  $\text{SO}_2$  uptake coefficient ( $\gamma_{\text{SO}_2}$ ) as a kinetic  
170 parameter to account for the particle size effects. Comprehensive calculation of  $\gamma_{\text{SO}_2}$  can be  
171 found in our previous studies (Gen et al., 2019a, b; Tang et al., 2023; Zhang et al., 2020a).

172 Aqueous-phase photochemical reactions were performed using a quartz photo reactor (Mabato  
173 et al., 2023; 2022). Specifically, a 500 mL solution containing 100 ppm bisulfite and 1 ppm BB  
174 TOC extracts were continuously mixed using a magnetic stirrer throughout the experiments.  
175 Note that the 1 ppm BB TOC and 100 ppm bisulfite align well with the atmospheric-relevant  
176 ranges in aqueous aerosols, fogs and clouds, where PS concentration can reach hundreds of  
177 micromolar and total sulfur concentration can exceed several millimolar (Anastasio et al., 1997;  
178 Guo et al., 2012; Shen et al., 2012; Rao and Collett, 1995). To achieve air-saturated conditions,  
179 synthetic air was continuously introduced to the solutions at a flow rate  $0.5 \text{ L min}^{-1}$  throughout  
180 the experiments. The above mixed solutions were then exposed to radiation via the same xenon  
181 lamp (light intensity of  $1318 \text{ mW/cm}^2$ ) as in the droplet experiments. Samples were collected  
182 at 1h interval for a total of 8 h for sulfate and bisulfite analysis using ion chromatography.  
183 Unlike droplet experiments, NaCl was not added to the bulk solution in most studies, unless  
184 specified otherwise.

## 185 **3 Results and Discussion**

### 186 **3.1 Enhanced sulfate production in BB-NaCl droplets over IS-NaCl droplets.**

187 As no sulfate was detected under dark conditions for any of the experiments, we have focused  
188 on the light experiments. Figure 1 depicts the sulfate production by (a) fresh BB-NaCl; (b) aged  
189 BB-NaCl droplets as a function of time in the presence of light, air, and  $\text{SO}_2$  at 80% RH. Our  
190 previous study (Tang et al., 2023) has found significantly higher sulfate formation of IS-NaCl  
191 droplets over NaCl droplets. Here, we only focus on the comparison of sulfate formation  
192 between different kinds of BB-NaCl droplets and IS-NaCl droplets. Regardless of whether the  
193 extracts were fresh or aged, the sulfate production by BB-NaCl droplets was higher than IS-  
194 NaCl droplets. Specifically, sulfate formed by fresh (F) BB-NaCl droplets followed the trends  
195 of  $\text{CS}_\text{F}\text{-NaCl}$  ( $16.8 \pm 2.6 \text{ mM ppmC}^{-1}$ )  $>$   $\text{RS}_\text{F}\text{-NaCl}$  ( $9.8 \pm 0.1 \text{ mM ppmC}^{-1}$ )  $>$   $\text{WS}_\text{F}\text{-NaCl}$  ( $4.2 \pm$   
196  $0.2 \text{ mM ppmC}^{-1}$ )  $>$   $\text{IS}_\text{F}\text{-NaCl}$  ( $0.8 \text{ mM ppmC}^{-1}$ ) after illumination for 1080 min. In aged (A)  
197 samples, while  $\text{BB}_\text{A}\text{-NaCl}$  is more efficient than  $\text{IS}_\text{A}\text{-NaCl}$  in sulfate formation, the order of  
198 sulfate formation was different from the fresh samples:  $\text{RS}_\text{A}\text{-NaCl}$  ( $35.2 \pm 0.6 \text{ mM ppmC}^{-1}$ )  $>$   
199  $\text{CS}_\text{A}\text{-NaCl}$  ( $13.0 \pm 0.1 \text{ mM ppmC}^{-1}$ )  $>$   $\text{WS}_\text{A}\text{-NaCl}$  ( $6.0 \pm 1.6 \text{ mM ppmC}^{-1}$ )  $>$   $\text{IS}_\text{A}\text{-NaCl}$  ( $0.6 \text{ mM}$

200 ppmC<sup>-1</sup>). The sulfate enhancement factors of RS<sub>F</sub>-NaCl, WS<sub>F</sub>-NaCl, and CS<sub>F</sub>-NaCl over IS<sub>F</sub>-  
 201 NaCl after 18 h SO<sub>2</sub> uptake (Sulfate<sub>BB<sub>F</sub>-NaCl</sub>/IS<sub>F</sub>-NaCl) were 11.7, 5.0 and 20.0, respectively.  
 202 The enhancement of sulfate can also be observed in aged BB samples, with values of 54.3, 9.2  
 203 and 20.1 for RS<sub>A</sub>-NaCl, WS<sub>A</sub>-NaCl, and CS<sub>A</sub>-NaCl, respectively. The lower sulfate formation  
 204 of IS-NaCl droplets than BB-NaCl droplets can be explained by the significantly higher TOC  
 205 concentration of IS due to the incomplete and smoldering combustion (Table S1). The TOC  
 206 concentration of the IS extracts (>550 mg L<sup>-1</sup>) was nearly an order of magnitude higher than  
 207 that of the BB extracts (34.0-69.9 mg L<sup>-1</sup>), and Σanions/WSOC exhibited a more than tenfold  
 208 increase in BB extracts than in IS extracts. Previous studies have confirmed that the smoldering  
 209 condition of BB results in significantly more organic compounds and less ions than flaming  
 210 condition (Wang et al., 2020b; Fushimi et al., 2017; Kalogridis et al., 2018; Kim et al., 2018).  
 211 Additionally, significantly higher polycyclic aromatic hydrocarbons (PAHs) proportion  
 212 (12.2%-16.6% by intensity) in BB than IS (~5.0%) were observed by GC×GC-MS. Huang et  
 213 al. (2022a) reported higher PAHs in BB particles (CS, WS, RS, >262.5 mg kg<sup>-1</sup>, >3.7% of  
 214 organic matter) than in IS particles (3.3 mg kg<sup>-1</sup>, 0.9% of organic matter) (Song et al., 2023).  
 215 Fushimi et al. (2017) and Kim et al. (2021) demonstrated that more PAHs would be emitted  
 216 under flaming than smoldering conditions. PAHs like pyrene, fluoranthene, and phenanthrene  
 217 have been recognized as PS (Jiang et al., 2021; Yang et al., 2021) and are mainly from  
 218 combustion processes, e.g., pyrosynthesis from aliphatic and aromatic precursors in biomass  
 219 burning processes and the constituents vary with temperatures and oxygen contents (Pozzoli et  
 220 al., 2004). The higher percentage of PAHs in BB together with the collection procedure (mixed  
 221 combustion and higher temperature for real BB and smoldering and lower temperature for IS)  
 222 suggested that the BB materials would generate more PAHs at high temperatures and may  
 223 contribute to sulfate formation.

224 Table 1 and Figure S2 present the reactive ( $\gamma_{SO_2}$ ) and normalized reactive SO<sub>2</sub> uptake  
 225 coefficients ( $n\gamma_{SO_2}$ ) of different BB-NaCl droplets. The  $\gamma_{SO_2}$  obtained in our study are 0.9 -  
 226  $6.6 \times 10^{-6}$ , which are consistent but fall on the low side of the reported heterogeneous SO<sub>2</sub>  
 227 oxidation processes, including nitrate photolysis ( $10^{-6}$ - $10^{-5}$ ) (Gen et al., 2019a), TMI-catalyzed  
 228 oxidation ( $10^{-6}$ - $10^{-4}$ ) (Zhang et al., 2024), NO<sub>2</sub>/O<sub>3</sub> oxidation ( $10^{-6}$ - $10^{-4}$ ) (Zhang et al., 2021a;  
 229 Zhang and Chan, 2023a) and peroxide oxidation ( $10^{-6}$ - $10^{-1}$ ) (Wang et al., 2021a; Ye et al., 2018;  
 230 Yao et al., 2019). Additionally, the reported  $\gamma_{SO_2}$  in our study aligns well with the results  
 231 obtained from ambient samples in Beijing (Zhang et al., 2020b). The large discrepancy of the  
 232 reported  $\gamma_{SO_2}$  can be attributed to the differences in aerosol components, particle size, RH, SO<sub>2</sub>  
 233 and oxidants concentrations. Higher  $n\gamma_{SO_2}$  were found for fresh and aged real BB-NaCl than  
 234 IS-NaCl droplets, following the trend of :CS<sub>F</sub>-NaCl ( $8.8 \times 10^{-8}$  ppmC<sup>-1</sup>)>RS<sub>F</sub>-NaCl ( $6.2 \times 10^{-8}$   
 235 ppmC<sup>-1</sup>)>WS<sub>F</sub>-NaCl ( $2.0 \times 10^{-8}$  ppmC<sup>-1</sup>)>IS<sub>F</sub>-NaCl ( $0.61 \times 10^{-8}$  ppmC<sup>-1</sup>) and RS<sub>A</sub>-NaCl ( $2.2 \times 10^{-7}$   
 236 ppmC<sup>-1</sup>)>CS<sub>A</sub>-NaCl ( $6.2 \times 10^{-8}$  ppmC<sup>-1</sup>)>WS<sub>A</sub>-NaCl ( $3.5 \times 10^{-8}$  ppmC<sup>-1</sup>)>IS<sub>A</sub>-NaCl ( $0.46 \times 10^{-8}$   
 237 ppmC<sup>-1</sup>), respectively.

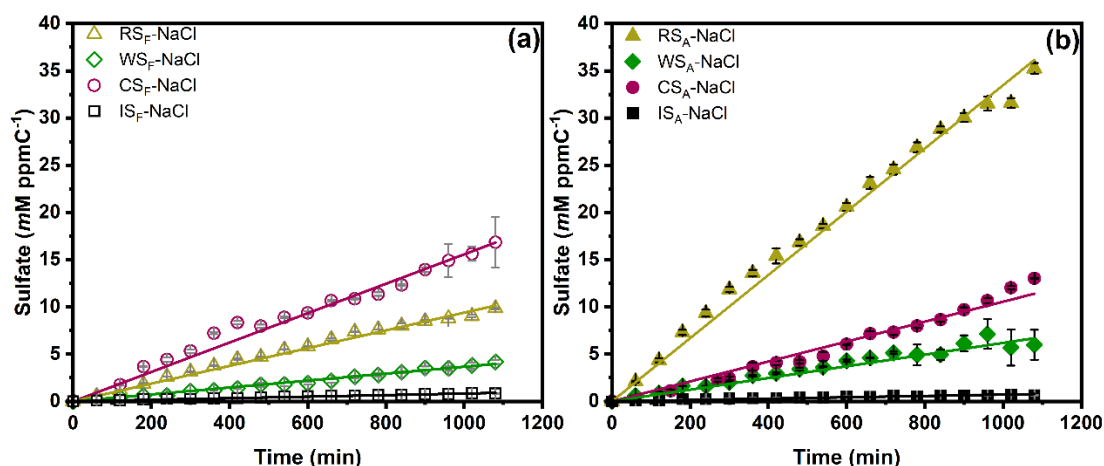
238 In our previous study, we observed a significant increase in sulfate formation in IS-NaCl  
 239 droplets than NaCl droplets, which we attributed to PS present in the IS (Tang et al., 2023).  
 240 Considering the fact that BB-NaCl droplets produced sulfate more efficiently than IS-NaCl  
 241 droplets and NaCl droplets, we explore the underlying mechanisms driving this phenomenon.  
 242 Possible reasons include nitrate (from BB extracts or newly formed) photolysis, [Cl-H<sub>3</sub>O<sup>+</sup>-O<sub>2</sub>]

243 photoexcitation ( $\text{Cl}^-$  from BB extracts),  $\text{H}_2\text{O}_2$  oxidation, BC-catalyzed oxidation, reactive  
244 nitrogen species oxidation, and organics-driven pathways e.g., HCHO, photosensitizing  
245 components, organic peroxide, and TMI-organic oxidation (Ye et al., 2023).

246 Since there was no nitrate peak in our Raman spectra in all experiments, the potential impact  
247 from nitrate photolysis was excluded. Besides, the significantly low  $\text{Cl}^-$  concentration (0.0002-  
248 0.001M) in the original BB extracts (compared to 1M NaCl, Table S1) has minimized the  
249 influence of chloride photoexcitation of  $[\text{Cl}^- \cdot \text{H}_3\text{O}^+ \cdot \text{O}_2]$  ( $\text{Cl}^-$  from BB extracts) on the sulfate  
250 formation. Reactive nitrogen species e.g.,  $\text{NO}_x$ , HONO and  $\text{NH}_3$  were neither introduced nor  
251 detected in our system, indicating that the oxidation pathway involving reactive nitrogen  
252 species was insignificant. Additionally, the water extraction process has excluded the possibility  
253 of BC-catalyzed oxidation. The absence of sulfate formation in dark conditions ruled out the  
254 involvement of direct  $\text{H}_2\text{O}_2$  oxidation and organic peroxide oxidation pathways. The  
255 concentrations of TMI did not exhibit a consistent relationship with the sulfate formation  
256 observed in both  $\text{BB}_F\text{-NaCl}$  and  $\text{BB}_A\text{-NaCl}$  droplets (Figure S3), suggesting that the TMI-  
257 catalyzed oxidation pathway may not be responsible for the observed phenomenon. Therefore,  
258 the most probable reason for the enhancement of sulfate formation by BB-NaCl droplets over  
259 NaCl droplets would be the photosensitizing components. Given the complexity and the lack  
260 of a method to quantify PS in BB aerosols, using the total TOC concentration as an upper limit  
261 for estimating PS concentration is considered a compromise that allows systematic comparison.  
262 The sulfate formation reported here can be considered as the lower limit of photosensitizing  
263 capacity. Our goal is to compare the photosensitizing ability in different chemical systems, but  
264 not to quantify their absolute values.

265  
266 State-of-the-art mass spectrometry analysis including UHPLC-Orbitrap-MS and GC $\times$ GC-MS  
267 showed the existence of possible PS such as PAHs (e.g., fluoranthene, pyrene,  
268 cyclopenta[cd]pyrene, 4-methylphenanthrene, benzo[a]pyrene, perylene, Table S2) and  
269 aromatic carbonyls (SyrAld, VL, 3,4-dimethoxybenzaldehyde, acetophenone, acetosyringone,  
270 Table S2). Photosensitizing components can directly or indirectly (by forming secondary  
271 oxidants in the presence of oxygen) oxidize S(IV) to S(VI). Wang et al. (2020a) proposed a  
272 direct oxidation process of S(IV) to sulfate by excited triplet states of photosensitizers ( $^3\text{PS}^*$ ).  
273 To explore the contribution of the direct  $^3\text{PS}^*$  oxidation on sulfate formation, we performed the  
274 same sets of experiments in  $\text{N}_2$ -saturated condition, shown in Figure S4. Under  $\text{N}_2$ -saturated  
275 conditions, secondary oxidants such as  $\text{HO}_2\cdot$ ,  $\text{OH}\cdot$  oxidation pathway can be ruled out due to  
276 the lack of oxygen. Chlorine radicals from droplets can also react with dissolved  $\text{SO}_2$  to  
277 generate sulfite radicals, but  $\text{O}_2$  is required to form sulfate. Despite initial molecular oxygen in  
278 the droplets may also participate in sulfate formation under  $\text{N}_2$ -saturated conditions, its  
279 contributions are likely minimal. Consequently, the sulfate formed under  $\text{N}_2$ -saturated condition  
280 can be considered as the upper limit of direct  $^3\text{PS}^*$  oxidation. The BB-NaCl droplets showed  
281 only direct  $\text{PS}^*$  oxidation contribution of 3.6% to 22.7%, highlighting the predominant role of  
282 secondary oxidants (Tang et al., 2023). For  $\text{BB}_F\text{-NaCl}$  droplets, the contribution of direct  $^3\text{PS}^*$   
283 followed the trend of  $\text{WS}_F\text{-NaCl}$  (22.7%) >  $\text{RS}_F\text{-NaCl}$  (15.7%) >  $\text{CS}_F\text{-NaCl}$  (7.0%), while for  
284  $\text{BB}_A\text{-NaCl}$  droplets,  $\text{WS}_A\text{-NaCl}$  (10.2%) >  $\text{CS}_A\text{-NaCl}$  (6.7%) >  $\text{RS}_A\text{-NaCl}$  (3.6%) was observed.  
285 In summary, regardless of whether fresh or aged, the secondary oxidants triggered by indirect  
286  $^3\text{PS}^*$  oxidation were the main reason for sulfate formation, highlighting the importance of  $\text{O}_2$

287 in <sup>3</sup>PS\* mediated oxidation processes.



288

289 Figure 1. Sulfate production under different droplet compositions as a function of time: (a) fresh  
 290 BB-NaCl droplets; (b) aged BB-NaCl droplets in air at 80% RH. RS, WS, CS and IS represent  
 291 rice straw, wheat straw, corn straw and incense burning, respectively. The subscripts F and A  
 292 represent fresh and aged, respectively.

293

294 Table 1. Sulfate formation rate ( $k_{SO_4^{2-}}$ ), reactive ( $\gamma_{SO_2}$ ) and normalized  $SO_2$  uptake coefficient  
 295 ( $n\gamma_{SO_2}$ ) at various particle compositions at 80% RH as well as sulfate formation rate ( $k_{SO_4^{2-}}$ )  
 296 using different BB extracts and model compounds in bulk aqueous reactions. 1, 10, 100 and  
 297 200 represent the concentration of different compounds (in ppm).

<b>Droplet Experiments</b>			
Particle Composition	$k_{SO_4^{2-}}$ ( $\mu\text{M min}^{-1} \text{ ppmC}^{-1}$ )	$\gamma_{SO_2}$	$n\gamma_{SO_2}$ <sup>a</sup> ppmC <sup>-1</sup>
RS <sub>F</sub> -NaCl	$9.4 \pm 0.10$	$(2.2 \pm 0.023) \times 10^{-6}$	$(6.2 \pm 0.066) \times 10^{-8}$
WS <sub>F</sub> -NaCl	$3.7 \pm 0.048$	$(0.66 \pm 0.0086) \times 10^{-6}$	$(2.0 \pm 0.027) \times 10^{-8}$
CS <sub>F</sub> -NaCl	$15.6 \pm 0.11$	$(2.0 \pm 0.015) \times 10^{-6}$	$(8.8 \pm 0.065) \times 10^{-8}$
IS <sub>F</sub> -NaCl	$0.83 \pm 0.011$	$(1.7 \pm 0.034) \times 10^{-6}$	$(0.61 \pm 0.012) \times 10^{-8}$
RS <sub>A</sub> -NaCl	$33.5 \pm 0.38$	$(6.6 \pm 0.074) \times 10^{-6}$	$(21.5 \pm 0.24) \times 10^{-8}$
WS <sub>A</sub> -NaCl	$6.2 \pm 0.18$	$(0.92 \pm 0.027) \times 10^{-6}$	$(3.5 \pm 0.10) \times 10^{-8}$
CS <sub>A</sub> -NaCl	$10.6 \pm 0.23$	$(1.0 \pm 0.023) \times 10^{-6}$	$(6.2 \pm 0.13) \times 10^{-8}$
IS <sub>A</sub> -NaCl	$0.72 \pm 0.026$	$(1.3 \pm 0.052) \times 10^{-6}$	$(0.46 \pm 0.017) \times 10^{-8}$
<b>Bulk Aqueous Experiments</b>			
Aqueous Reactions	Concentration (ppm)	$k_{SO_4^{2-}}$	$k_{SO_4^{2-}}$



		(ppm min <sup>-1</sup> )	(μM min <sup>-1</sup> )
RS <sub>F</sub>	1	0.31	3.2
RS <sub>F</sub> -NaCl	1-100	0.16	1.6
RS <sub>F</sub> -NaCl	1-200	0.085	0.9
WS <sub>F</sub>	1	0.19	2.0
CS <sub>F</sub>	1	0.25	2.6
IS <sub>F</sub>	1	0.19	2.0
RS <sub>A</sub>	1	0.33	3.4
RS <sub>A</sub> -NaCl	1-100	0.37	3.8
RS <sub>A</sub> -NaCl	1-200	0.63	6.4
WS <sub>A</sub>	1	0.26	2.7
CS <sub>A</sub>	1	0.33	3.4
IS <sub>A</sub>	1	0.080	0.82
NaCl	100	0.051	0.52
NaCl	200	0.079	0.81
SyrAld	1	0.15	1.5
SyrAld-Pyz	1-1	0.68	7.1
SyrAld-Pyz-NaCl	1-1-10	0.67	6.9
SyrAld-Pyz-NaCl	1-1-100	0.55	5.7
SyrAld-Pyz-NaCl	1-1-200	0.50	5.2
SyrAld-4-NC	1-1	0.11	1.1
SyrAld-4-NC- NaCl	1-1-10	0.13	1.4
SyrAld-4-NC- NaCl	1-1-100	0.13	1.4
SyrAld-4-NC- NaCl	1-1-200	0.15	1.5
SyrAld-NaCl	1-10	0.11	1.1
SyrAld-NaCl	1-100	0.17	1.8
SyrAld-NaCl	1-200	0.17	1.7
VL	1	0.26	2.7
VL-Pyz	1-10	0.61	6.4

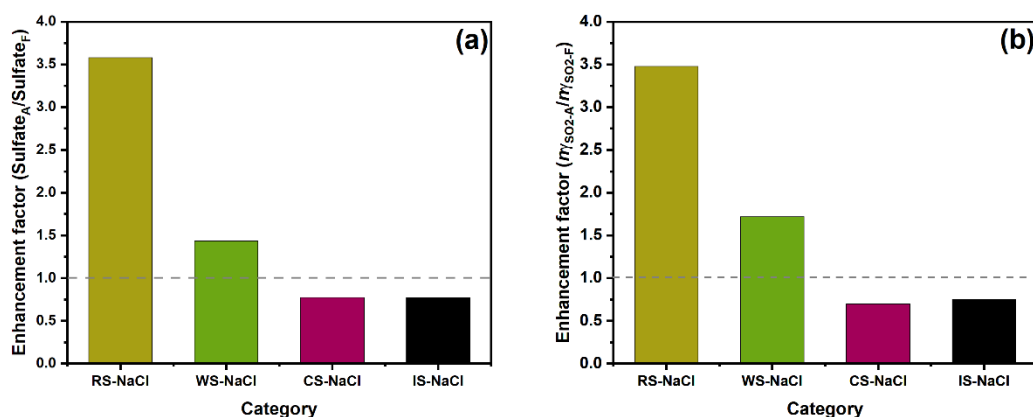
VL-Pyz-NaCl	1-1-10	0.55	5.8
VL-Pyz-NaCl	1-1-100	0.43	4.5
VL-Pyz-NaCl	1-1-200	0.42	4.3
VL-4-NC	1-1	0.17	1.7
VL-4-NC-NaCl	1-1-10	0.22	2.3
VL-4-NC-NaCl	1-1-100	0.27	2.7
VL-4-NC-NaCl	1-1-200	0.23	2.4
VL-NaCl	1-10	0.25	2.6
VL-NaCl	1-100	0.26	2.7
VL-NaCl	1-200	0.28	2.9

<sup>a</sup>The  $n\gamma_{SO_2}$  was calculated by normalizing the  $\gamma_{SO_2}$  with the TOC concentration in the BB extracts, i.e.,  $n\gamma_{SO_2} = \gamma_{SO_2}/TOC$

298

### 299 3.2 Aging effects on sulfate formation across various BB materials

300 To investigate the aging effects across various BB materials on sulfate formation, we subjected  
 301 the collected BB filters to OH radical aging by irradiating them with UV lights at wavelengths  
 302 of 185 nm and 254 nm. This combination effectively generate OH radicals (Tang et al., 2023).  
 303 Figure S5 exhibits the differences in sulfate formation rates in droplets of different fresh and  
 304 aged BB materials. RS and WS show sulfate formation enhancement, while CS and IS show  
 305 reduction after aging. Figure 2(a) shows that the 18h sulfate enhancement factor  
 306 ( $Sulfate_A/Sulfate_F$ ) followed the trend of RS-NaCl (3.6) > WS-NaCl (1.4) > CS-NaCl (0.8)  $\approx$  IS-  
 307 NaCl (0.8), which is neither consistent with the trends of sulfate formation for  $BB_F$ -NaCl nor  
 308  $BB_A$ -NaCl, indicating the varying effects of aging of BB materials. A similar trend was found  
 309 for  $n\gamma_{SO_2}$ , showing the highest and lowest sulfate enhancement for RS-NaCl (3.5) and IS-NaCl  
 310 (0.7), respectively.



311

312 Figure 2. Enhancement factor of (a) sulfate and (b) normalized SO<sub>2</sub> uptake coefficient  $n\gamma_{SO_2}$   
 313 between fresh and aged BB-NaCl droplets.

314 Bulk aqueous reactions using fresh/aged BB extracts without NaCl were performed to  
315 investigate the aging effects on the sulfate formation in the cloud phase (Figure S6). As the  
316 experiment proceeded, sulfate concentrations accumulated while bisulfite concentrations  
317 decreased. Concurrently, the pH of the aqueous solution decreased from approximately 5.0 to  
318 3.0, reflecting enhanced acidity. Bulk reactions showed lower sulfate formation rates than  
319 droplets reactions, which may be attributed to the accelerated reactions induced by PS at the  
320 air-water interface (Wang et al., 2024c; Martins-Costa et al., 2022), as well as the differences  
321 in concentrations of S(IV) and NaCl between bulk and droplet surfaces. However, given that  
322 interfacial reactions are closely linked to particle size (Wei et al., 2020; Chen et al., 2022b), and  
323 additional research is needed to better understand its influence. Our experiments involve large  
324 droplets of the size of 60  $\mu\text{m}$ . The interfacial effects of such large droplets may not be evident.  
325 Future work to examine the interfacial effects of submicron and nanometer size particles is  
326 needed.

### 327 **3.3 Chemical characterization of BB extracts and sulfate formation in bulk aqueous** 328 **solutions**

329 In bulk experiments, all BB extracts have higher  $k_{\text{SO}_4^{2-}}$  after aging. The increased sulfate  
330 formation of BB extracts after aging may be due to changes in their chemical compositions.  
331 Compared to  $\text{RS}_\text{F}$  (28.3% for CHON- and 67.3% for CHN+ in total intensity),  $\text{RS}_\text{A}$  has higher  
332 CHON- (36.1%) and CHN+ (88.3%) percentages (Figs. S7-S8). Zhao et al. (2022) observed a  
333 slight increase in CHON percentage for RS from 53.4% to 56.2% after aging. Similar trend was  
334 observed for CS extracts, where CHON- and CHN+ percentage increases from 26.7% and 65.2%  
335 to 31.5% and 68.8%, respectively, after aging. To semi-qualitatively distinguish BrC  
336 chromophores from the rest of dissolved organic carbon, we used the DBE value to the range  
337 of  $0.5\text{C} \leq \text{DBE} \leq 0.9\text{C}$  as a criterion (Lin et al., 2018). For example,  $\text{RS}_{\text{A-BrC}}$  denotes the BrC  
338 chromophores in  $\text{RS}_\text{A}$ , according to the above. Larger intensity fractions of CHON- species  
339 were found in  $\text{RS}_{\text{A-BrC}}$  (41.9%) and  $\text{CS}_{\text{A-BrC}}$  (35.5%) than  $\text{RS}_{\text{F-BrC}}$  (32.3%) and  $\text{CS}_{\text{F-BrC}}$  (34.7%).  
340 One of the key categories of CHON- is nitrated aromatics, which have been widely identified  
341 in lab-generated BB smoke (Huang et al., 2022b; Wang et al., 2017a; Zhang et al., 2022; Xie et  
342 al., 2019) and field campaigns (Salvador et al., 2020; Mohr et al., 2013; Chen et al., 2022a). A  
343 series of CHON- species, e.g.,  $\text{C}_6\text{H}_5\text{NO}_3$ ,  $\text{C}_6\text{H}_5\text{NO}_4$ ,  $\text{C}_7\text{H}_7\text{NO}_3$ , and  $\text{C}_8\text{H}_9\text{NO}_3$ , which were  
344 tentatively identified as nitrophenol, nitrocatechol, methyl-nitrophenol, and dimethyl-  
345 nitrophenol, have been detected in our BB extracts. Nitrophenols photolysis has been found to  
346 be a potential source of OH radicals (Sangwan and Zhu, 2018; Guo and Li, 2023; Cheng et al.,  
347 2009; Sangwan and Zhu, 2016) and it may partially contribute to the increase in sulfate  
348 formation by  $\text{RS}_\text{A}$  and  $\text{CS}_\text{A}$ .

349 Approximately 80% of the CHN+ species identified exhibited a diatomic nitrogen composition  
350 in their molecular formula. The precise determination of the molecular structures of these  
351 compounds solely based on elemental composition is challenging due to the presence of stable  
352 isomers. However, the N-bases, which contain two nitrogen atoms, can be attributed to various  
353 N-heterocyclic alkaloids (Figure S9). For example, homologs of  $\text{C}_5\text{H}_6\text{N}_2(\text{CH}_2)_n$  were likely  
354 pyrazine, pyrimidine or amino pyridine, which were composed of six-membered heterocyclic  
355 rings with N atoms and alkyl side chains (Lin et al., 2012; Laskin et al., 2009).  $\text{C}_5\text{H}_8\text{N}_2(\text{CH}_2)_n$

356 were likely alkyl-substituted imidazole compounds, featuring a five-membered heterocyclic  
357 ring with two nitrogen atoms as the core structure and alkyl side chains (Lin et al., 2012; Laskin  
358 et al., 2009). For  $C_7H_6N_2(CH_2)_n$  homologs, the core skeleton was  $C_7H_6N_2$ , with an  $AI_{mod}$  of 0.8,  
359 indicating its distinctive characteristics of compounds containing fused five-membered and six-  
360 membered rings, such as benzimidazole or indazole (Wang et al., 2017b). Redox-inactive  
361 heterocyclic nitrogen-containing bases, e.g., pyridine, imidazole, and their derivatives, have  
362 been shown to enhance the redox activity of humic-like substances (HULIS) fraction by  
363 hydrogen-atom transfer, with the degree of enhancement directly correlated to their  
364 concentration (Dou et al., 2015; Kipp et al., 2004). Thus, the increased  $CHN^+$  percentage may  
365 also contribute to the enhanced sulfate formation of  $RS_A$  and  $CS_A$  by acting as a H-bond  
366 acceptor to facilitate the  $^3PS^*$ -mediated oxidation by generating more oxidants.

367 However, the  $CHON^-$  and  $CHN^+$  percentages in  $WS_A$  were lower than  $WS_F$ , indicating that the  
368 sulfate enhancement in  $WS_A$  was not due to the  $CHON^-$  and  $CHN^+$  species. Instead,  $CHO^-$   
369 accounted for higher proportion in  $WS_A$  (68.5%) and  $WS_{A-BrC}$  (68.9%) than  $WS_F$  (65.0%) and  
370  $WS_{F-BrC}$  (64.8%). This aligns with a prior AMS study, showing increased  $CHO^-$  proportions in  
371 aged wheat burning emissions (Fang et al., 2017). We suppose that  $CHO^-$  compounds,  
372 particularly photosensitizing compounds with carbonyl groups, would explain the difference of  
373 sulfate formation in  $WS$  extracts (Gómez Alvarez et al., 2012; Mabato et al., 2023; Felber et al.,  
374 2020; Fu et al., 2015). Therefore, we filtered the chemical formula of  $CHO^-$  species from  
375 UHPLC-Orbitrap-HRMS by applying the maximum carbonyl ratio (MCR) (Zhang et al., 2021b;  
376 Wang et al., 2024a; Calderon-Arrieta et al., 2024; Liu et al., 2023a),  $H/C$ ,  $O/C$  as well as  
377 modified aromaticity index ( $AI_{mod}$ ) to focus on potential PS (Zherebker et al., 2022; Koch and  
378 Dittmar, 2006). In short, molecular formula were classified into six groups, namely, condensed  
379 aromatics ( $AI_{mod} \geq 0.67$ ), polyphenolics ( $0.50 < AI_{mod} < 0.67$ ), highly unsaturated and phenolic  
380 compounds ( $AI_{mod} \leq 0.5$ ,  $H/C < 1.5$ ), aliphatics ( $H/C \geq 1.5$ ,  $O/C \leq 0.9$ ,  $N=0$ ), peptide-like  
381 compounds ( $H/C \geq 1.5$ ,  $O/C \leq 0.9$ ,  $N > 0$ ) and sugar-like compounds ( $H/C \geq 1.5$ ,  $O/C > 0.9$ ), details  
382 can be found in Text S1. As aliphatics, peptide-like compounds and sugar-like compounds are  
383 unlikely to be PS, we exclude them as potential PS. By applying further data filtration involving  
384  $CHO^-$ , condensed aromatics, polyphenolics, highly unsaturated and phenolic compounds based  
385 on the aforementioned criteria, as well as  $MCR \geq 0.9$  (which includes oxidized unsaturated and  
386 highly unsaturated compounds such as PS like imidazole-carboxaldehyde and PAHs) (Zhang et  
387 al., 2021b), 52.6% and 49.7% of the compounds (by intensity) can be considered as potential  
388 PS in  $WS_A$  and  $WS_F$ , respectively. The main compositional difference lies in polyphenolics,  
389 comprising 26.3% and 21.8% of  $WS_A$  and  $WS_F$  respectively. Therefore, the higher sulfate  
390 formation in  $WS_A$  may be related to the higher contributions of the polyphenolics, e.g.,  $C_8H_8O_3$ .

391 To summarize, we propose that in aqueous reactions, the enhanced sulfate formation in  $CS_A$   
392 and  $RS_A$  was likely due to the increased proportions (by intensity) of  $CHON^-$  and  $CHN^+$  species,  
393 potentially nitrophenols and N-heterocyclic compounds. Conversely, the increased sulfate  
394 formation in  $WS_A$  appears to be linked to a higher percentage of  $CHO^-$  species. However, the  
395 association between detailed chemical characteristics and sulfate formation is not available in  
396 this study due to the complexity of the interactions between different chemical categories and  
397 difficulties in the interpretation of the coefficients. Future studies are needed to elucidate the  
398 relationships between sulfate formation and the chemical characteristics.

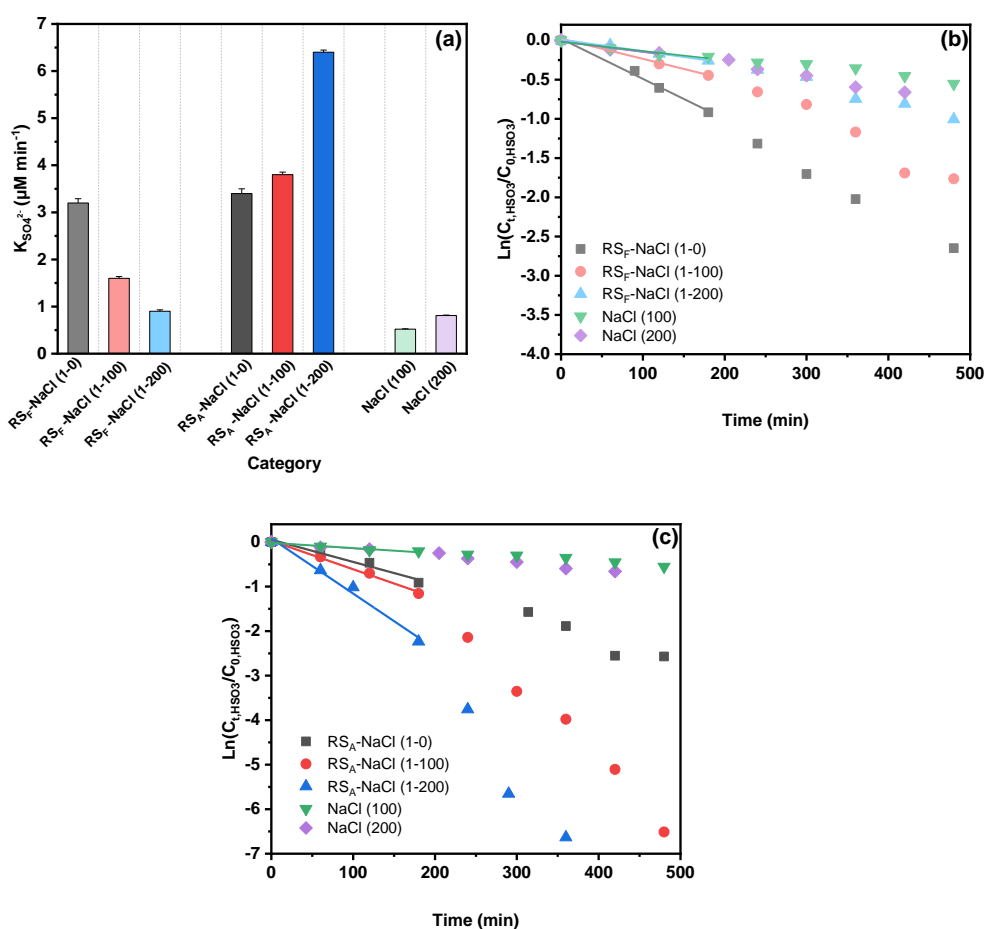
### 399 3.4 Effects of Chloride and Nitrogen-containing Species on Sulfate Formation

400 Unlike the droplet experiments where RS-NaCl has the highest sulfate enhancement factor after  
401 aging, aqueous reaction results (without NaCl) show a sulfate enhancement trend of  
402 WS>CS>RS>IS, suggesting that chloride may take effect in the droplet experiments, especially  
403 in RS-NaCl system. To evaluate the effects of chloride on sulfate formation, we conducted bulk  
404 reaction experiments using RS extracts as an example with 100-200 ppm NaCl additions, where  
405 the NaCl to TOC ratio ranged from 100:1 to 200:1 to match the 100:1 to 1000:1 range in droplet  
406 experiments. Interestingly, incorporating NaCl yielded contrasting results for RS<sub>F</sub> and RS<sub>A</sub>  
407 (Figure 3). While the addition of NaCl enhanced sulfate formation in RS<sub>A</sub>, it showed the  
408 opposite trend in RS<sub>F</sub>. The nature of the cations and ionic strength may affect the sulfate  
409 formation rate; however, previous studies have indicated that their effects are negligible (Zhang  
410 and Chan, 2024; Parker and Mitch, 2016). The opposite effect of the NaCl addition on RS<sub>F</sub> and  
411 RS<sub>A</sub>, to some extent, explains the significantly higher sulfate and SO<sub>2</sub> uptake coefficient  
412 enhancement factor for RS-NaCl in Fig. 2. Compared to the RS-based system, NaCl control  
413 experiment showed minimum (but non-zero) sulfate formation (Table 1 and Figure 3). On one  
414 hand, it supported the findings that chloride participated in the sulfate formation under light but  
415 no sulfate formation under dark (Cao et al., 2024; Tang et al., 2023; Zhang and Chan, 2024).  
416 On the other hand, the opposite trend of Cl<sup>-</sup> effects on RS<sub>F</sub> and RS<sub>A</sub> reflects its complex  
417 interactions with BB extracts under light and air. While direct reaction between S(IV) species  
418 and <sup>3</sup>PS\* may occur (Wang et al., 2020a), other pathways, i.e., interactions among halide ions,  
419 PS and oxygen should also be considered. Detailed mechanisms will be discussed later.

420 Statistical analysis using the Spearman correlation coefficients, as guided by the Shapiro-Wilk  
421 test (Table S4), revealed that the CHO, CHON, and CHN species exhibited significant  
422 correlations ( $|R|>0.7$ ) with the sulfate formation rate ( $p < 0.01$ , Figure S10). While PS can be  
423 the main CHO species contributing to sulfate formation, N-containing organic compounds  
424 (NOCs), i.e., CHN and CHON species, may affect the chloride contribution to the sulfate  
425 formation rate. Therefore, we selected SyrAld and VL as model CHO (PS), pyrazine (Pyz) as a  
426 model CHN, and 4-nitrocatechol (4-NC) as a model CHON to elucidate how the N containing  
427 species can alter the effects of chloride on sulfate formation rate by studying the CHO+Cl<sup>-</sup>,  
428 CHO+CHN+Cl<sup>-</sup>, and CHO+CHON+Cl<sup>-</sup> systems. For SyrAld and VL, as the [Cl<sup>-</sup>]<sub>0</sub>/[PS]<sub>0</sub>  
429 increases,  $k_{SO_4^{2-}}$  initially decreases and then increases. The initial decrease of  $k_{SO_4^{2-}}$  may be  
430 attributed to the quenching of <sup>3</sup>PS\* by electron transfer from Cl<sup>-</sup> or loss of OH radicals by  
431 forming ClOH• through reaction of OH•+Cl<sup>-</sup> ↔ ClOH• (Anastasio and Newberg, 2007).  
432 Excessive chloride (e.g. 100 and 200 ppm) may generate Cl and OH radicals through  
433 photoexcitation in the presence of air and water and compensate for the loss of <sup>3</sup>PS\* or OH  
434 radicals. Previous studies have shown contradicting influence of halides on the photosensitized  
435 oxidation of organic compounds or bisulfite. Parker and Mitch (2016) and Zhang et al. (2023)  
436 attributed the significantly higher photodegradation of dienes, thioethers and acetaminophen to  
437 the formation of reactive halogen species generated by the reactions of PS and halides. Zhang  
438 and Chan (2024) reported that [Cl<sup>-</sup>/PS]<sub>0</sub> in the range of 1:2 to 4:1 did not lead to significant  
439 difference in sulfate formation. The differences between the current results and the  
440 aforementioned study might be attributed to the higher [Cl<sup>-</sup>/PS]<sub>0</sub> used in this study (up to 200:1)  
441 which may have been sufficient to initiate the relevant reactions, as well as the difference in

442 photosensitizing capacities of the PS studied (triplet quantum yield of  $0.86 \pm 0.05$  for 2-IC and  
 443  $0.21 \pm 0.01$  for VL) (Felber et al., 2021; 2020). Safiarian et al. (2023) reported that increasing  
 444 chloride concentrations facilitated anthracene photosensitization by producing high-level  
 445 reactive oxygen species (ROS). Wang et al. (2023a) found that the effects of chloride on sulfate  
 446 formation depended on the specific PS: enhancing sulfate production for benzophenone (BP)  
 447 and 3,4-dimethoxybenzaldehyde (DMB), but decreasing it for 1,4-naphthoquinone.

448 Incorporating CHN species yielded a 2-3-fold increase in  $k_{SO_4^{2-}}$ , due to the enhanced H transfer  
 449 by CHN acting as H-bond acceptor (Dou et al., 2015). With the addition of NaCl, the enhanced  
 450 H-transfer effect by CHN was inhibited, possibly due to the consumption of  $^3PS^*$  by Cl $^-$ . On  
 451 the other hand, the addition of model CHON species into PS decreased  $k_{SO_4^{2-}}$ , due to the  
 452 consumption of  $^3PS^*$  by CHON species, in agreement with Wang et al. (2023b) who reported  
 453 increased effective quantum yield of 4-NC under co-photolysis with VL. Further addition of  
 454 NaCl increased the  $k_{SO_4^{2-}}$ , possibly due to the consumption of 4-NC by RCS (Wang et al.,  
 455 2024b), which, to some extent, reduced the loss of  $^3PS^*$ . Generally, the addition of chloride  
 456 increased  $k_{SO_4^{2-}}$  of PS-CHON but decreased  $k_{SO_4^{2-}}$  of PS-CHN. However, the ambient air is  
 457 characterized by the presence of tens of thousands of chemical compounds. As a result, the  
 458 interplay among this diverse array of species may occur in ways that exceed current  
 459 understanding, necessitating additional research to investigate the interactions between  
 460 different organic compounds more thoroughly.



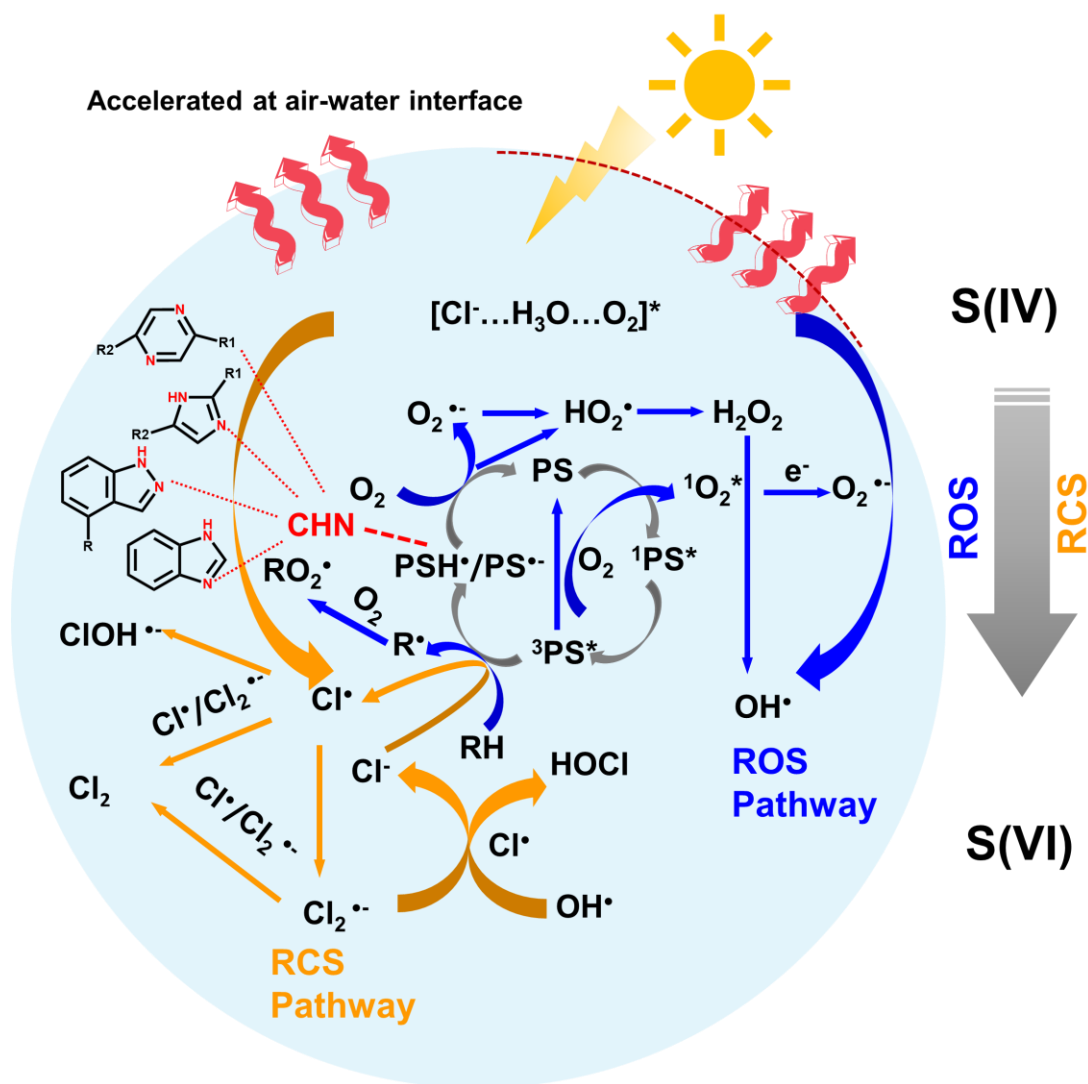
461

462 Figure 3. (a) Sulfate formation rate and (b) (c) bisulfite decay in RS-NaCl aqueous reactions. 1-0,  
463 1-100, and 1-200 refer to the concentration ratios of  $\text{TOC}_{\text{RS}}$  and NaCl, in which 1, 100, 200 represent  
464 1 ppm, 100 ppm and 200 ppm, respectively.

### 465 3.5 Proposed mechanism for sulfate formation

466 A conceptual diagram of PS and chloride mediated ROS and RCS production in the oxidation  
467 of S (IV) to S (VI) was shown in Fig. 4. Initially, the PS (e.g., SyrAld and VL) absorb solar  
468 radiation and produce the singlet state  $^1\text{PS}^*$ , which then undergoes a spin conversion through  
469 intersystem crossing, leading to the formation of the triplet state  $^3\text{PS}^*$ . The  $^3\text{PS}^*$  can react with  
470 molecular oxygen through energy transfer and generate singlet state  $^1\text{O}_2^*$ , while the  $^3\text{PS}^*$  returns  
471 to ground state. The  $^1\text{O}_2^*$  can then transform to  $\text{O}_2^{\cdot-}$  via electron transfer. The  $^3\text{PS}^*$  can also react  
472 with an H donor (RH, e.g., organic acids, syringol, guaiacol, Table S3), leading to the formation  
473 of alkyl or phenoxy radical ( $\text{R}^{\cdot}$ ) and a ketyl radical ( $\text{PSH}^{\cdot}$ ).  $\text{R}^{\cdot}$  can react with  $\text{O}_2$  and form  $\text{RO}_2$   
474 radicals while  $\text{PSH}^{\cdot}$  can transfer an H atom to  $\text{O}_2$  and form  $\text{HO}_2^{\cdot}$ , returning to its ground state  
475 PS. Additionally,  $^3\text{PS}^*$  can react with an electron donor, e.g.,  $\text{Cl}^-$ , and form chlorine radicals  
476 and  $\text{PS}^{\cdot-}$ . The formed  $\text{PS}^{\cdot-}$  then reacts with  $\text{O}_2$  and form  $\text{O}_2^{\cdot-}$ , which undergoes a series of  
477 reactions and form  $\text{HO}_2^{\cdot}$ ,  $\text{H}_2\text{O}_2$  and  $\text{OH}^{\cdot}$ . The above-mentioned reactions are the main processes  
478 in the ROS pathway. Recently, Zhang and Chan(2024) have proposed that the reactive chlorine  
479 species (RCS) would contribute to sulfate formation. Cao et al. (2024) proposed a mechanism  
480 of OH and Cl radicals formation by  $[\text{Cl}^- \text{-H}_3\text{O}^+ \text{-O}_2]$  under light irradiation through an electron  
481 transfer process. Our results also demonstrate that the addition of  $\text{Cl}^-$  will affect the oxidation  
482 process of S(VI) (Figures 3, S11-S13). Combining the above, the RCS pathway was shown in  
483 yellow arrows in Figure 4. The  $\text{Cl}^{\cdot}$  can be formed in two pathways, photoexcitation of the  $[\text{Cl}^-$   
484  $\text{-H}_3\text{O}^+ \text{-O}_2]$  complex that generates Cl radicals in deliquescent BB-NaCl droplets or aqueous  
485 BB-NaCl solution (Cao et al., 2024), and  $\text{PS}^*$  mediated  $\text{Cl}^{\cdot}$  formation via electron transfer by  
486  $\text{Cl}^-$  (Corral Arroyo et al., 2019). The formed  $\text{Cl}^{\cdot}$  can then react with each other through radical-  
487 radical reactions and produce molecular  $\text{Cl}_2$ . The  $\text{Cl}^{\cdot}$  can also react with  $\text{Cl}^-$  or  $\text{Cl}_2^{\cdot-}$ , forming  
488  $\text{Cl}_2^{\cdot-}$  or  $\text{Cl}_2$ .  $\text{Cl}^{\cdot}$  and  $\text{Cl}_2^{\cdot-}$  can also react with OH and form HOCl.  $^3\text{PS}^*$  itself can also oxidize  
489 the S(IV) (e.g., dissolved  $\text{SO}_2$  or bisulfite) to S(VI). However, significantly lower sulfate  
490 formation was found in the presence of  $\text{N}_2$  than air (Figure S4), highlighting the importance of  
491 secondary oxidants compared to direct  $\text{PS}^*$  oxidation. As a consequence, these reactive species,  
492 e.g.,  $\text{OH}^{\cdot}/\text{HO}_2^{\cdot}/\text{O}_2^{\cdot-}$  and  $\text{Cl}^{\cdot}/\text{Cl}_2^{\cdot-}$  may all participate in the oxidation of S(IV) to S(VI). In  
493 addition, nitrogen-containing heterocyclic compounds such as pyrazine can act as H-bonding  
494 acceptor and facilitate the H transfer, which then generates more ROS (Dou et al., 2015). Note  
495 that although ROS and RCS pathways both contribute to the oxidation from S(IV) to S(VI),  
496 they may act as competitive relationships due to the co-consumption of  $\text{PS}^*$ . Therefore,  
497 different Cl effects may occur regarding various combinations of reactants (Figure 3, promoting  
498 effect in  $\text{RS}_{\text{A}}$ , inhibiting effects on  $\text{RS}_{\text{F}}$ ).

499



500

501 Figure 4. Conceptual diagram of PS and chloride-mediated ROS and RCS production, in the  
502 oxidation processes from S(IV) to S(VI)

#### 503 **4 Atmospheric Implication**

504 This study provided laboratory evidence that the PS in biomass burning extracts can enhance  
505 the sulfate formation in NaCl particles, primarily by triggering the formation of secondary  
506 oxidants under light and air, with less contribution of direct photosensitization via triplets  
507 (evidenced by N<sub>2</sub> atmosphere, Figure S4). The sulfate formation rates of BB<sub>F</sub>-NaCl particles  
508 were ~10 folds higher than that of IS<sub>F</sub>-NaCl, following the trends of CS<sub>F</sub>-NaCl>RS<sub>F</sub>-  
509 NaCl>WS<sub>F</sub>-NaCl>IS<sub>F</sub>-NaCl. Upon UV exposure, the sulfate formation trends shifted to RS<sub>A</sub>-  
510 NaCl>CS<sub>A</sub>-NaCl>WS<sub>A</sub>-NaCl>IS<sub>A</sub>-NaCl, which might be explained by the effects of chloride  
511 (evidenced by aqueous reactions, Figure 3 and Table 1). Interestingly, the incorporation of Cl<sup>-</sup>  
512 into bulk solutions increased the sulfate formation rate in RS<sub>A</sub>, while decreased it in RS<sub>F</sub>. This  
513 seems to be different from our group's previous work where no significant sulfate formation  
514 rate was found with the addition of Cl<sup>-</sup> (Zhang and Chan, 2024). The difference can be explained  
515 by the following reasons: 1) differences in PS/Cl<sup>-</sup>, the prior study might have used an



516 insufficient PS/Cl<sup>-</sup> ratio (2:1-1:4) while the current one significantly expanded it to 1:200. 2)  
517 differences in photosensitizing capacity: the former study used a strong PS, while the current  
518 study focused on the real BB (using TOC as a metric, with only a small portion of TOC  
519 considered as PS). 3) the complexity of the reaction system, the former study focused on mixing  
520 two individual species, while in real BB extracts, more complicated reactions may occur.  
521 Furthermore, our results using model PS show that although additional model CHN species  
522 would increase the sulfate formation by expedited H transfer via acting as H-bond acceptor, the  
523 addition of chloride could inhibit the sulfate formation rate, suggesting that the RCS pathway  
524 was less efficient in sulfate formation compared to ROS pathway in PS-CHN bulk system  
525 (Figure S11 and S12).

526 While our prior study has examined the potential interplay between chloride and PS at limited  
527 mixing ratios (up to 4:1 in bulk solution) (Zhang and Chan, 2024), this work expanded the Cl<sup>-</sup>  
528 /PS ratio to a broader range (200:1) and systematically identified the interactions among  
529 different organics, including PS, NOCs, and chloride, using sulfate formation as a compass.  
530 This highlights the importance of studying secondary aerosol formation in mixed experimental  
531 systems under air pollution complex. Our work suggests that in coastal regions heavily  
532 influenced by anthropogenic emissions like biomass burning, especially those near the rice-  
533 growing regions or affected by transported wildfire smoke, such as Guangdong, Fujian and  
534 Taiwan, the transported BB plumes together with the high RH (Cheung et al., 2015) and  
535 abundant reactive gases, would play an important role in sulfate and potentially secondary  
536 organic aerosol formation.

#### 537 **Data availability**

538 Datasets are available upon request to the corresponding author, Chak K. Chan  
539 (chak.chan@kaust.edu.sa).

#### 540 **Author contributions**

541 RT and CC conceptualized and designed the study. YQ and YC collected the samples. RT  
542 performed the experiments, data analysis and wrote the draft. JM provided assistance in data  
543 processing. All the authors reviewed, edited and contributed to the scientific discussions.

#### 544 **Competing interests**

545 The authors declare no conflicts of interest.

#### 546 **Acknowledgments**

547 We gratefully acknowledge the support from the Hong Kong Research Grants Council (No.  
548 11314222), the National Natural Science Foundation of China (42107115), and the Natural  
549 Science Foundation of Shandong Province, China (ZR2021QD111). The authors also thank the  
550 University Research Facility in Chemical and Environmental Analysis (UCEA) at The Hong  
551 Kong Polytechnic University for the use of its UHPLC-HESI-Orbitrap Mass Spectrometer and  
552 Dr Sirius Tse and Dr Chi Hang Chow for assistance with sample analyses. CKC also  
553 acknowledged the support from the KAUST baseline research fund (BAS/1/1432-01-01)

554 and KAUST Center of Excellence for Smart Health (KCSH) fund (Award number  
555 5932).

## 556 **References**

557 Alexander, B., Allman, D. J., Amos, H. M., Fairlie, T. D., Dachs, J., Hegg, D. A., and Sletten, R. S.:  
558 Isotopic constraints on the formation pathways of sulfate aerosol in the marine boundary layer of  
559 the subtropical northeast Atlantic Ocean, *Journal of Geophysical Research: Atmospheres*, 117,  
560 <https://doi.org/10.1029/2011JD016773>, 2012.

561 Anastasio, C. and Newberg, J. T.: Sources and sinks of hydroxyl radical in sea-salt particles, *Journal*  
562 *of Geophysical Research: Atmospheres*, 112, 2007.

563 Andreae, M. O.: Emission of trace gases and aerosols from biomass burning – an updated  
564 assessment, *Atmos. Chem. Phys.*, 19, 8523-8546, 10.5194/acp-19-8523-2019, 2019.

565 Bond, T. C., Doherty, S. J., Fahey, D. W., Forster, P. M., Berntsen, T., DeAngelo, B. J., Flanner, M. G.,  
566 Ghan, S., Kärcher, B., Koch, D., Kinne, S., Kondo, Y., Quinn, P. K., Sarofim, M. C., Schultz, M. G.,  
567 Schulz, M., Venkataraman, C., Zhang, H., Zhang, S., Bellouin, N., Guttikunda, S. K., Hopke, P. K.,  
568 Jacobson, M. Z., Kaiser, J. W., Klimont, Z., Lohmann, U., Schwarz, J. P., Shindell, D., Storelvmo, T.,  
569 Warren, S. G., and Zender, C. S.: Bounding the role of black carbon in the climate system: A  
570 scientific assessment, *Journal of Geophysical Research: Atmospheres*, 118, 5380-5552,  
571 <https://doi.org/10.1002/jgrd.50171>, 2013.

572 Cai, J., Zeng, X., Zhi, G., Gligorovski, S., Sheng, G., Yu, Z., Wang, X., and Peng, P.: Molecular  
573 composition and photochemical evolution of water-soluble organic carbon (WSOC) extracted  
574 from field biomass burning aerosols using high-resolution mass spectrometry, *Atmos. Chem. Phys.*,  
575 20, 6115-6128, 10.5194/acp-20-6115-2020, 2020.

576 Calderon-Arrieta, D., Morales, A. C., Hettiyadura, A. P. S., Estock, T. M., Li, C., Rudich, Y., and Laskin,  
577 A.: Enhanced Light Absorption and Elevated Viscosity of Atmospheric Brown Carbon through  
578 Evaporation of Volatile Components, *Environmental Science & Technology*, 58, 7493-7504,  
579 10.1021/acs.est.3c10184, 2024.

580 Cao, Y., Liu, J., Ma, Q., Zhang, C., Zhang, P., Chen, T., Wang, Y., Chu, B., Zhang, X., Francisco, J. S.,  
581 and He, H.: Photoactivation of Chlorine and Its Catalytic Role in the Formation of Sulfate Aerosols,  
582 *Journal of the American Chemical Society*, 146, 1467-1475, 10.1021/jacs.3c10840, 2024.

583 Chen, J., Li, C., Ristovski, Z., Milic, A., Gu, Y., Islam, M. S., Wang, S., Hao, J., Zhang, H., He, C., Guo,  
584 H., Fu, H., Miljevic, B., Morawska, L., Thai, P., Lam, Y. F., Pereira, G., Ding, A., Huang, X., and Dumka,  
585 U. C.: A review of biomass burning: Emissions and impacts on air quality, health and climate in  
586 China, *Science of The Total Environment*, 579, 1000-1034,  
587 <https://doi.org/10.1016/j.scitotenv.2016.11.025>, 2017.

588 Chen, Y., Zheng, P., Wang, Z., Pu, W., Tan, Y., Yu, C., Xia, M., Wang, W., Guo, J., Huang, D., Yan, C.,  
589 Nie, W., Ling, Z., Chen, Q., Lee, S., and Wang, T.: Secondary Formation and Impacts of Gaseous  
590 Nitro-Phenolic Compounds in the Continental Outflow Observed at a Background Site in South  
591 China, *Environmental Science & Technology*, 56, 6933-6943, 10.1021/acs.est.1c04596, 2022a.

592 Chen, Z., Liu, P., Wang, W., Cao, X., Liu, Y.-X., Zhang, Y.-H., and Ge, M.: Rapid Sulfate Formation  
593 via Uncatalyzed Autoxidation of Sulfur Dioxide in Aerosol Microdroplets, *Environmental Science &*  
594 *Technology*, 56, 7637-7646, 10.1021/acs.est.2c00112, 2022b.

595 Cheng, S.-B., Zhou, C.-H., Yin, H.-M., Sun, J.-L., and Han, K.-L.: OH produced from o-nitrophenol  
596 photolysis: A combined experimental and theoretical investigation, *The Journal of chemical physics*,

597 130, 2009.

598 Cheung, H. H., Yeung, M. C., Li, Y. J., Lee, B. P., and Chan, C. K.: Relative humidity-dependent  
599 HTDMA measurements of ambient aerosols at the HKUST supersite in Hong Kong, China, *Aerosol*  
600 *Science and Technology*, 49, 643-654, 2015.

601 Chi, J. W., Li, W. J., Zhang, D. Z., Zhang, J. C., Lin, Y. T., Shen, X. J., Sun, J. Y., Chen, J. M., Zhang, X.  
602 Y., Zhang, Y. M., and Wang, W. X.: Sea salt aerosols as a reactive surface for inorganic and organic  
603 acidic gases in the Arctic troposphere, *Atmos. Chem. Phys.*, 15, 11341-11353, 10.5194/acp-15-  
604 11341-2015, 2015.

605 Corral Arroyo, P., Aellig, R., Alpert, P. A., Volkamer, R., and Ammann, M.: Halogen activation and  
606 radical cycling initiated by imidazole-2-carboxaldehyde photochemistry, *Atmospheric Chemistry*  
607 *and Physics*, 19, 10817-10828, 2019.

608 Dou, J., Lin, P., Kuang, B.-Y., and Yu, J. Z.: Reactive Oxygen Species Production Mediated by Humic-  
609 like Substances in Atmospheric Aerosols: Enhancement Effects by Pyridine, Imidazole, and Their  
610 Derivatives, *Environmental Science & Technology*, 49, 6457-6465, 10.1021/es5059378, 2015.

611 Fang, Z., Deng, W., Zhang, Y., Ding, X., Tang, M., Liu, T., Hu, Q., Zhu, M., Wang, Z., Yang, W., Huang,  
612 Z., Song, W., Bi, X., Chen, J., Sun, Y., George, C., and Wang, X.: Open burning of rice, corn and  
613 wheat straws: primary emissions, photochemical aging, and secondary organic aerosol formation,  
614 *Atmos. Chem. Phys.*, 17, 14821-14839, 10.5194/acp-17-14821-2017, 2017.

615 Felber, T., Schaefer, T., and Herrmann, H.: Five-Membered Heterocycles as Potential  
616 Photosensitizers in the Tropospheric Aqueous Phase: Photophysical Properties of Imidazole-2-  
617 carboxaldehyde, 2-Furaldehyde, and 2-Acetylfuran, *The Journal of Physical Chemistry A*, 124,  
618 10029-10039, 10.1021/acs.jpca.0c07028, 2020.

619 Felber, T., Schaefer, T., He, L., and Herrmann, H.: Aromatic Carbonyl and Nitro Compounds as  
620 Photosensitizers and Their Photophysical Properties in the Tropospheric Aqueous Phase, *The*  
621 *Journal of Physical Chemistry A*, 125, 5078-5095, 10.1021/acs.jpca.1c03503, 2021.

622 Fu, H., Ciuraru, R., Dupart, Y., Passananti, M., Tinel, L., Rossignol, S., Perrier, S., Donaldson, D. J.,  
623 Chen, J., and George, C.: Photosensitized Production of Atmospherically Reactive Organic  
624 Compounds at the Air/Aqueous Interface, *Journal of the American Chemical Society*, 137, 8348-  
625 8351, 10.1021/jacs.5b04051, 2015.

626 Fushimi, A., Saitoh, K., Hayashi, K., Ono, K., Fujitani, Y., Villalobos, A. M., Shelton, B. R., Takami, A.,  
627 Tanabe, K., and Schauer, J. J.: Chemical characterization and oxidative potential of particles emitted  
628 from open burning of cereal straws and rice husk under flaming and smoldering conditions,  
629 *Atmospheric Environment*, 163, 118-127, <https://doi.org/10.1016/j.atmosenv.2017.05.037>, 2017.

630 Gantt, B. and Meskhidze, N.: The physical and chemical characteristics of marine primary organic  
631 aerosol: a review, *Atmos. Chem. Phys.*, 13, 3979-3996, 10.5194/acp-13-3979-2013, 2013.

632 Gen, M., Zhang, R., Huang, D. D., Li, Y., and Chan, C. K.: Heterogeneous SO<sub>2</sub> Oxidation in Sulfate  
633 Formation by Photolysis of Particulate Nitrate, *Environmental Science & Technology Letters*, 6, 86-  
634 91, 10.1021/acs.estlett.8b00681, 2019a.

635 Gen, M., Zhang, R., Huang, D. D., Li, Y., and Chan, C. K.: Heterogeneous Oxidation of SO<sub>2</sub> in Sulfate  
636 Production during Nitrate Photolysis at 300 nm: Effect of pH, Relative Humidity, Irradiation  
637 Intensity, and the Presence of Organic Compounds, *Environmental Science & Technology*, 53,  
638 8757-8766, 10.1021/acs.est.9b01623, 2019b.

639 Gómez Alvarez, E., Wortham, H., Strekowski, R., Zetzsch, C., and Gligorovski, S.: Atmospheric  
640 Photosensitized Heterogeneous and Multiphase Reactions: From Outdoors to Indoors,

641 Environmental Science & Technology, 46, 1955-1963, 10.1021/es2019675, 2012.

642 Guo, S. and Li, H.: Photolysis of nitrophenols in gas phase and aqueous environment: a potential  
643 daytime source for atmospheric nitrous acid (HONO), Environmental Science: Atmospheres, 3,  
644 143-155, 2023.

645 Hu, W., Zhou, H., Chen, W., Ye, Y., Pan, T., Wang, Y., Song, W., Zhang, H., Deng, W., Zhu, M., Wang,  
646 C., Wu, C., Ye, C., Wang, Z., Yuan, B., Huang, S., Shao, M., Peng, Z., Day, D. A., Campuzano-Jost, P.,  
647 Lambe, A. T., Worsnop, D. R., Jimenez, J. L., and Wang, X.: Oxidation Flow Reactor Results in a  
648 Chinese Megacity Emphasize the Important Contribution of S/IVOCs to Ambient SOA Formation,  
649 Environmental Science & Technology, 56, 6880-6893, 10.1021/acs.est.1c03155, 2022.

650 Huang, G., Wang, S., Chang, X., Cai, S., Zhu, L., Li, Q., and Jiang, J.: Emission factors and chemical  
651 profile of I/SVOCs emitted from household biomass stove in China, Science of The Total  
652 Environment, 842, 156940, <https://doi.org/10.1016/j.scitotenv.2022.156940>, 2022a.

653 Huang, R.-J., Yang, L., Shen, J., Yuan, W., Gong, Y., Ni, H., Duan, J., Yan, J., Huang, H., You, Q., and  
654 Li, Y. J.: Chromophoric Fingerprinting of Brown Carbon from Residential Biomass Burning,  
655 Environmental Science & Technology Letters, 9, 102-111, 10.1021/acs.estlett.1c00837, 2022b.

656 Huang, S., Wu, Z., Poulain, L., van Pinxteren, M., Merkel, M., Assmann, D., Herrmann, H., and  
657 Wiedensohler, A.: Source apportionment of the organic aerosol over the Atlantic Ocean from  
658 53°&thinsp;N to 53°&thinsp;S: significant contributions from marine emissions and long-range  
659 transport, Atmos. Chem. Phys., 18, 18043-18062, 10.5194/acp-18-18043-2018, 2018.

660 Jammoul, A., Dumas, S., D'Anna, B., and George, C.: Photoinduced oxidation of sea salt halides by  
661 aromatic ketones: a source of halogenated radicals, Atmos. Chem. Phys., 9, 4229-4237,  
662 10.5194/acp-9-4229-2009, 2009.

663 Jiang, H., Carena, L., He, Y., Wang, Y., Zhou, W., Yang, L., Luan, T., Li, X., Brigante, M., Vione, D., and  
664 Gligorovski, S.: Photosensitized Degradation of DMSO Initiated by PAHs at the Air-Water Interface,  
665 as an Alternative Source of Organic Sulfur Compounds to the Atmosphere, Journal of Geophysical  
666 Research: Atmospheres, 126, e2021JD035346, <https://doi.org/10.1029/2021JD035346>, 2021.

667 Jones, M. W., Abatzoglou, J. T., Veraverbeke, S., Andela, N., Lasslop, G., Forkel, M., Smith, A. J. P.,  
668 Burton, C., Betts, R. A., van der Werf, G. R., Sitch, S., Canadell, J. G., Santín, C., Kolden, C., Doerr, S.  
669 H., and Le Quéré, C.: Global and Regional Trends and Drivers of Fire Under Climate Change,  
670 Reviews of Geophysics, 60, e2020RG000726, <https://doi.org/10.1029/2020RG000726>, 2022.

671 Kalogridis, A. C., Popovicheva, O. B., Engling, G., Diapouli, E., Kawamura, K., Tachibana, E., Ono, K.,  
672 Kozlov, V. S., and Eleftheriadis, K.: Smoke aerosol chemistry and aging of Siberian biomass burning  
673 emissions in a large aerosol chamber, Atmospheric Environment, 185, 15-28,  
674 <https://doi.org/10.1016/j.atmosenv.2018.04.033>, 2018.

675 Kim, Y. H., Warren, S. H., Krantz, Q. T., King, C., Jaskot, R., Preston, W. T., George, B. J., Hays, M. D.,  
676 Landis, M. S., and Higuchi, M.: Mutagenicity and lung toxicity of smoldering vs. flaming emissions  
677 from various biomass fuels: implications for health effects from wildland fires, Environmental health  
678 perspectives, 126, 017011, 2018.

679 Kim, Y. H., Warren, S. H., Kooter, I., Williams, W. C., George, I. J., Vance, S. A., Hays, M. D., Higuchi,  
680 M. A., Gavett, S. H., DeMarini, D. M., Jaspers, I., and Gilmour, M. I.: Chemistry, lung toxicity and  
681 mutagenicity of burn pit smoke-related particulate matter, Particle and Fibre Toxicology, 18, 45,  
682 10.1186/s12989-021-00435-w, 2021.

683 Kipp, B. H., Faraj, C., Li, G., and Njus, D.: Imidazole facilitates electron transfer from organic  
684 reductants, Bioelectrochemistry, 64, 7-13, <https://doi.org/10.1016/j.bioelechem.2003.12.010>, 2004.

685 Koch, B. P. and Dittmar, T.: From mass to structure: An aromaticity index for high-resolution mass  
686 data of natural organic matter, *Rapid communications in mass spectrometry*, 20, 926-932, 2006.

687 Laskin, A., Laskin, J., and Nizkorodov, S. A.: Chemistry of Atmospheric Brown Carbon, *Chemical*  
688 *Reviews*, 115, 4335-4382, 10.1021/cr5006167, 2015.

689 Laskin, A., Smith, J. S., and Laskin, J.: Molecular Characterization of Nitrogen-Containing Organic  
690 Compounds in Biomass Burning Aerosols Using High-Resolution Mass Spectrometry,  
691 *Environmental Science & Technology*, 43, 3764-3771, 10.1021/es803456n, 2009.

692 Li, F., Zhou, S., Zhao, J., Hang, J., Lu, H., Li, X., Gao, M., Li, Y., and Wang, X.: Aqueous  
693 Photosensitization of Syringaldehyde: Reactivity, Effects of Environmental Factors, and Formation  
694 of Brown Carbon Products, *ACS Earth and Space Chemistry*, 2024.

695 Li, S., Jiang, X., Roveretto, M., George, C., Liu, L., Jiang, W., Zhang, Q., Wang, W., Ge, M., and Du,  
696 L.: Photochemical aging of atmospherically reactive organic compounds involving brown carbon  
697 at the air-aqueous interface, *Atmos. Chem. Phys.*, 19, 9887-9902, 10.5194/acp-19-9887-2019,  
698 2019.

699 Liang, Z., Li, Y., Go, B. R., and Chan, C. K.: Complexities of Photosensitization in Atmospheric  
700 Particles, *ACS ES&T Air*, 10.1021/acsestair.4c00112, 2024.

701 Lin, P., Rincon, A. G., Kalberer, M., and Yu, J. Z.: Elemental Composition of HULIS in the Pearl River  
702 Delta Region, China: Results Inferred from Positive and Negative Electrospray High Resolution  
703 Mass Spectrometric Data, *Environmental Science & Technology*, 46, 7454-7462,  
704 10.1021/es300285d, 2012.

705 Lin, P., Fleming, L. T., Nizkorodov, S. A., Laskin, J., and Laskin, A.: Comprehensive Molecular  
706 Characterization of Atmospheric Brown Carbon by High Resolution Mass Spectrometry with  
707 Electrospray and Atmospheric Pressure Photoionization, *Analytical Chemistry*, 90, 12493-12502,  
708 10.1021/acs.analchem.8b02177, 2018.

709 Liu, D., Zhang, Y., Zhong, S., Chen, S., Xie, Q., Zhang, D., Zhang, Q., Hu, W., Deng, J., Wu, L., Ma,  
710 C., Tong, H., and Fu, P.: Large differences of highly oxygenated organic molecules (HOMs) and  
711 low-volatile species in secondary organic aerosols (SOAs) formed from ozonolysis of  $\beta$ -pinene  
712 and limonene, *Atmos. Chem. Phys.*, 23, 8383-8402, 10.5194/acp-23-8383-2023, 2023a.

713 Liu, H., Pei, X., Zhang, F., Song, Y., Kuang, B., Xu, Z., and Wang, Z.: Relative Humidity Dependence  
714 of Growth Factor and Real Refractive Index for Sea Salt/Malonic Acid Internally Mixed Aerosols,  
715 *Journal of Geophysical Research: Atmospheres*, 128, e2022JD037579,  
716 <https://doi.org/10.1029/2022JD037579>, 2023b.

717 Liu, Y., Wang, T., Fang, X., Deng, Y., Cheng, H., Nabi, I., and Zhang, L.: Brown carbon: An underlying  
718 driving force for rapid atmospheric sulfate formation and haze event, *Science of the Total*  
719 *Environment*, 734, 139415, 2020.

720 Mabato, B. R. G., Li, Y. J., Huang, D. D., Wang, Y., and Chan, C. K.: Comparison of aqueous secondary  
721 organic aerosol (aqSOA) product distributions from guaiacol oxidation by non-phenolic and  
722 phenolic methoxybenzaldehydes as photosensitizers in the absence and presence of ammonium  
723 nitrate, *Atmos. Chem. Phys.*, 23, 2859-2875, 10.5194/acp-23-2859-2023, 2023.

724 Mabato, B. R. G., Lyu, Y., Ji, Y., Li, Y. J., Huang, D. D., Li, X., Nah, T., Lam, C. H., and Chan, C. K.:  
725 Aqueous secondary organic aerosol formation from the direct photosensitized oxidation of vanillin  
726 in the absence and presence of ammonium nitrate, *Atmos. Chem. Phys.*, 22, 273-293,  
727 10.5194/acp-22-273-2022, 2022.

728 Mao, J., Ren, X., Brune, W. H., Olson, J. R., Crawford, J. H., Fried, A., Huey, L. G., Cohen, R. C., Heikes,

729 B., Singh, H. B., Blake, D. R., Sachse, G. W., Diskin, G. S., Hall, S. R., and Shetter, R. E.: Airborne  
730 measurement of OH reactivity during INTEX-B, *Atmos. Chem. Phys.*, 9, 163-173, 10.5194/acp-9-  
731 163-2009, 2009.

732 Martins-Costa, M. T., Anglada, J. M., Francisco, J. S., and Ruiz-López, M. F.: Photosensitization  
733 mechanisms at the air–water interface of aqueous aerosols, *Chemical science*, 13, 2624-2631, 2022.

734 Mohr, C., Lopez-Hilfiker, F. D., Zotter, P., Prévôt, A. S. H., Xu, L., Ng, N. L., Herndon, S. C., Williams,  
735 L. R., Franklin, J. P., Zahniser, M. S., Worsnop, D. R., Knighton, W. B., Aiken, A. C., Gorkowski, K. J.,  
736 Dubey, M. K., Allan, J. D., and Thornton, J. A.: Contribution of Nitrated Phenols to Wood Burning  
737 Brown Carbon Light Absorption in Detling, United Kingdom during Winter Time, *Environmental  
738 Science & Technology*, 47, 6316-6324, 10.1021/es400683v, 2013.

739 Parker, K. M. and Mitch, W. A.: Halogen radicals contribute to photooxidation in coastal and  
740 estuarine waters, *Proceedings of the National Academy of Sciences*, 113, 5868-5873, 2016.

741 Peng, Z. and Jimenez, J. L.: Radical chemistry in oxidation flow reactors for atmospheric chemistry  
742 research, *Chemical Society Reviews*, 49, 2570-2616, 2020.

743 Pozzoli, L., Gilardoni, S., Perrone, M. G., de Gennaro, G., de Rienzo, M., and Vione, D.: POLYCYCLIC  
744 AROMATIC HYDROCARBONS IN THE ATMOSPHERE: MONITORING, SOURCES, SINKS AND FATE.  
745 I: MONITORING AND SOURCES, *Annali di Chimica*, 94, 17-33,  
746 <https://doi.org/10.1002/adic.200490002>, 2004.

747 Qin, Y., Wang, H., Wang, Y., Lu, X., Tang, H., Zhang, J., Li, L., and Fan, S.: Wildfires in Southeast Asia  
748 pollute the atmosphere in the northern South China Sea, *Science Bulletin*, 69, 1011-1015,  
749 <https://doi.org/10.1016/j.scib.2024.02.026>, 2024.

750 Qiu, Y., Wu, X., Zhang, Y., Xu, L., Hong, Y., Chen, J., Chen, X., and Deng, J.: Aerosol light absorption  
751 in a coastal city in Southeast China: Temporal variations and implications for brown carbon, *Journal  
752 of Environmental Sciences*, 80, 257-266, <https://doi.org/10.1016/j.jes.2019.01.002>, 2019.

753 Rowe, J. P., Lambe, A. T., and Brune, W. H.: Technical Note: Effect of varying the  $\lambda = 185$  and  
754  $254\text{ nm}$  photon flux ratio on radical generation in oxidation flow reactors, *Atmos. Chem.  
755 Phys.*, 20, 13417-13424, 10.5194/acp-20-13417-2020, 2020.

756 Ruiz-Lopez, M. F., Francisco, J. S., Martins-Costa, M. T. C., and Anglada, J. M.: Molecular reactions  
757 at aqueous interfaces, *Nature Reviews Chemistry*, 4, 459-475, 10.1038/s41570-020-0203-2, 2020.

758 Safarian, M. S., Ugboya, A., Khan, I., Marichev, K. O., and Grant, K. B.: New Insights into the  
759 Phototoxicity of Anthracene-Based Chromophores: The Chloride Salt Effect, *Chemical Research in  
760 Toxicology*, 36, 1002-1020, 10.1021/acs.chemrestox.2c00235, 2023.

761 Salvador, C. M. G., Tang, R., Priestley, M., Li, L. J., Tsiligiannis, E., Le Breton, M., Zhu, W., Zeng, L.,  
762 Wang, H., and Yu, Y.: Ambient nitro-aromatic compounds–biomass burning versus secondary  
763 formation in rural China, *Atmospheric Chemistry and Physics Discussions*, 2020, 1-36, 2020.

764 Sangwan, M. and Zhu, L.: Absorption cross sections of 2-nitrophenol in the 295–400 nm region  
765 and photolysis of 2-nitrophenol at 308 and 351 nm, *The Journal of Physical Chemistry A*, 120,  
766 9958-9967, 2016.

767 Sangwan, M. and Zhu, L.: Role of Methyl-2-nitrophenol Photolysis as a Potential Source of OH  
768 Radicals in the Polluted Atmosphere: Implications from Laboratory Investigation, *The Journal of  
769 Physical Chemistry A*, 122, 1861-1872, 10.1021/acs.jpca.7b11235, 2018.

770 Song, J., Li, M., Zou, C., Cao, T., Fan, X., Jiang, B., Yu, Z., Jia, W., and Peng, P. a.: Molecular  
771 Characterization of Nitrogen-Containing Compounds in Humic-like Substances Emitted from  
772 Biomass Burning and Coal Combustion, *Environmental Science & Technology*, 56, 119-130,

773 10.1021/acs.est.1c04451, 2022.

774 Song, K., Tang, R., Li, A., Wan, Z., Zhang, Y., Gong, Y., Lv, D., Lu, S., Tan, Y., Yan, S., Yan, S., Zhang,  
775 J., Fan, B., Chan, C. K., and Guo, S.: Particulate organic emissions from incense-burning smoke:  
776 Chemical compositions and emission characteristics, *Science of The Total Environment*, 897,  
777 165319, <https://doi.org/10.1016/j.scitotenv.2023.165319>, 2023.

778 Tang, R., Zhang, R., Ma, J., Song, K., Mabato, B. R. G., Cuevas, R. A. I., Zhou, L., Liang, Z., Vogel, A.  
779 L., Guo, S., and Chan, C. K.: Sulfate Formation by Photosensitization in Mixed Incense Burning–  
780 Sodium Chloride Particles: Effects of RH, Light Intensity, and Aerosol Aging, *Environmental Science  
781 & Technology*, 57, 10295-10307, 10.1021/acs.est.3c02225, 2023.

782 Teich, M., van Pinxteren, D., Kecorius, S., Wang, Z., and Herrmann, H.: First quantification of  
783 imidazoles in ambient aerosol particles: potential photosensitizers, brown carbon constituents, and  
784 hazardous components, *Environmental science & technology*, 50, 1166-1173, 2016.

785 Ting, Y., Mitchell, E. J. S., Allan, J. D., Liu, D., Spracklen, D. V., Williams, A., Jones, J. M., Lea-Langton,  
786 A. R., McFiggans, G., and Coe, H.: Mixing State of Carbonaceous Aerosols of Primary Emissions  
787 from “Improved” African Cookstoves, *Environmental Science & Technology*, 52, 10134-10143,  
788 10.1021/acs.est.8b00456, 2018.

789 Tkacik, D. S., Lambe, A. T., Jathar, S., Li, X., Presto, A. A., Zhao, Y., Blake, D., Meinardi, S., Jayne, J. T.,  
790 Croteau, P. L., and Robinson, A. L.: Secondary Organic Aerosol Formation from in-Use Motor  
791 Vehicle Emissions Using a Potential Aerosol Mass Reactor, *Environmental Science & Technology*,  
792 48, 11235-11242, 10.1021/es502239v, 2014.

793 van Pinxteren, M., Fiedler, B., van Pinxteren, D., Iinuma, Y., Körtzinger, A., and Herrmann, H.:  
794 Chemical characterization of sub-micrometer aerosol particles in the tropical Atlantic Ocean:  
795 marine and biomass burning influences, *Journal of Atmospheric Chemistry*, 72, 105-125,  
796 10.1007/s10874-015-9307-3, 2015.

797 Wang, K., Zhang, Y., Tong, H., Han, J., Fu, P., Huang, R.-J., Zhang, H., and Hoffmann, T.: Molecular-  
798 Level Insights into the Relationship between Volatility of Organic Aerosol Constituents and PM2.5  
799 Air Pollution Levels: A Study with Ultrahigh-Resolution Mass Spectrometry, *Environmental Science  
800 & Technology*, 58, 7947-7957, 10.1021/acs.est.3c10662, 2024a.

801 Wang, N., Zhou, D., Liu, H., Tu, Y., Ma, Y., and Li, Y.: Triplet-Excited Dissolved Organic Matter  
802 Efficiently Promoted Atmospheric Sulfate Production: Kinetics and Mechanisms, *Separations*, 10,  
803 335, 2023a.

804 Wang, S., Liu, T., Jang, J., Abbatt, J. P. D., and Chan, A. W. H.: Heterogeneous interactions between  
805 SO<sub>2</sub> and organic peroxides in submicron aerosol, *Atmos. Chem. Phys.*, 21, 6647-6661,  
806 10.5194/acp-21-6647-2021, 2021a.

807 Wang, T., Deng, L., Tan, C., Hu, J., and Singh, R. P.: Comparative analysis of chlorinated disinfection  
808 byproducts formation from 4-nitrophenol and 2-amino-4-nitrophenol during UV/post-  
809 chlorination, *Science of The Total Environment*, 927, 172200,  
810 <https://doi.org/10.1016/j.scitotenv.2024.172200>, 2024b.

811 Wang, W., Liu, Y., Wang, T., Ge, Q., Li, K., Liu, J., You, W., Wang, L., Xie, L., Fu, H., Chen, J., and  
812 Zhang, L.: Significantly Accelerated Photosensitized Formation of Atmospheric Sulfate at the Air–  
813 Water Interface of Microdroplets, *Journal of the American Chemical Society*, 146, 6580-6590,  
814 10.1021/jacs.3c11892, 2024c.

815 Wang, X., Gemayel, R., Baboian, V. J., Li, K., Boreave, A., Dubois, C., Tomaz, S., Perrier, S.,  
816 Nizkorodov, S. A., and George, C.: Naphthalene-derived secondary organic aerosols interfacial

817 photosensitizing properties, *Geophysical Research Letters*, 48, e2021GL093465, 2021b.

818 Wang, X., Gu, R., Wang, L., Xu, W., Zhang, Y., Chen, B., Li, W., Xue, L., Chen, J., and Wang, W.:  
819 Emissions of fine particulate nitrated phenols from the burning of five common types of biomass,  
820 *Environmental Pollution*, 230, 405-412, <https://doi.org/10.1016/j.envpol.2017.06.072>, 2017a.

821 Wang, X., Gemayel, R., Hayeck, N., Perrier, S., Charbonnel, N., Xu, C., Chen, H., Zhu, C., Zhang, L.,  
822 Wang, L., Nizkorodov, S. A., Wang, X., Wang, Z., Wang, T., Mellouki, A., Riva, M., Chen, J., and  
823 George, C.: Atmospheric Photosensitization: A New Pathway for Sulfate Formation, *Environmental*  
824 *Science & Technology*, 54, 3114-3120, 10.1021/acs.est.9b06347, 2020a.

825 Wang, Y., Hu, M., Xu, N., Qin, Y., Wu, Z., Zeng, L., Huang, X., and He, L.: Chemical composition and  
826 light absorption of carbonaceous aerosols emitted from crop residue burning: influence of  
827 combustion efficiency, *Atmos. Chem. Phys.*, 20, 13721-13734, 10.5194/acp-20-13721-2020,  
828 2020b.

829 Wang, Y., Qiu, T., Zhang, C., Hao, T., Mabato, B. R. G., Zhang, R., Gen, M., Chan, M. N., Huang, D.  
830 D., and Ge, X.: Co-photolysis of mixed chromophores affects atmospheric lifetimes of brown  
831 carbon, *Environmental Science: Atmospheres*, 3, 1145-1158, 2023b.

832 Wang, Y., Hu, M., Lin, P., Guo, Q., Wu, Z., Li, M., Zeng, L., Song, Y., Zeng, L., Wu, Y., Guo, S., Huang,  
833 X., and He, L.: Molecular Characterization of Nitrogen-Containing Organic Compounds in Humic-  
834 like Substances Emitted from Straw Residue Burning, *Environmental Science & Technology*, 51,  
835 5951-5961, 10.1021/acs.est.7b00248, 2017b.

836 Wei, Z., Li, Y., Cooks, R. G., and Yan, X.: Accelerated reaction kinetics in microdroplets: Overview  
837 and recent developments, *Annual Review of Physical Chemistry*, 71, 31-51, 2020.

838 Wu, C.-H., Yuan, C.-S., Yen, P.-H., Yeh, M.-J., and Soong, K.-Y.: Diurnal and seasonal variation,  
839 chemical characteristics, and source identification of marine fine particles at two remote islands in  
840 South China Sea: A superimposition effect of local emissions and long-range transport,  
841 *Atmospheric Environment*, 270, 118889, <https://doi.org/10.1016/j.atmosenv.2021.118889>, 2022.

842 Xie, M., Chen, X., Hays, M. D., and Holder, A. L.: Composition and light absorption of N-containing  
843 aromatic compounds in organic aerosols from laboratory biomass burning, *Atmos. Chem. Phys.*,  
844 19, 2899-2915, 10.5194/acp-19-2899-2019, 2019.

845 Yang, M., Zhang, H., Chang, F., and Hu, X.: Self-sensitized photochlorination of benzo[a]pyrene in  
846 saline water under simulated solar light irradiation, *Journal of Hazardous Materials*, 408, 124445,  
847 <https://doi.org/10.1016/j.jhazmat.2020.124445>, 2021.

848 Yao, M., Zhao, Y., Hu, M., Huang, D., Wang, Y., Yu, J. Z., and Yan, N.: Multiphase reactions between  
849 secondary organic aerosol and sulfur dioxide: kinetics and contributions to sulfate formation and  
850 aerosol aging, *Environmental Science & Technology Letters*, 6, 768-774, 2019.

851 Ye, C., Lu, K., Song, H., Mu, Y., Chen, J., and Zhang, Y.: A critical review of sulfate aerosol formation  
852 mechanisms during winter polluted periods, *Journal of Environmental Sciences*, 123, 387-399,  
853 <https://doi.org/10.1016/j.jes.2022.07.011>, 2023.

854 Ye, J., Abbatt, J. P., and Chan, A. W.: Novel pathway of SO<sub>2</sub> oxidation in the atmosphere: reactions  
855 with monoterpene ozonolysis intermediates and secondary organic aerosol, *Atmospheric*  
856 *Chemistry and Physics*, 18, 5549-5565, 2018.

857 You, B., Li, S., Tsona, N. T., Li, J., Xu, L., Yang, Z., Cheng, S., Chen, Q., George, C., Ge, M., and Du, L.:  
858 Environmental Processing of Short-Chain Fatty Alcohols Induced by Photosensitized Chemistry of  
859 Brown Carbons, *ACS Earth and Space Chemistry*, 4, 631-640,  
860 10.1021/acsearthspacechem.0c00023, 2020.



861 Zhang, L., Hu, B., Liu, X., Luo, Z., Xing, R., Li, Y., Xiong, R., Li, G., Cheng, H., Lu, Q., Shen, G., and Tao,  
862 S.: Variabilities in Primary N-Containing Aromatic Compound Emissions from Residential Solid Fuel  
863 Combustion and Implications for Source Tracers, *Environmental Science & Technology*, 56, 13622-  
864 13633, 10.1021/acs.est.2c03000, 2022.

865 Zhang, R. and Chan, C. K.: Simultaneous formation of sulfate and nitrate via co-uptake of SO<sub>2</sub>  
866 and NO<sub>2</sub> by aqueous NaCl droplets: combined effect of nitrate photolysis and chlorine chemistry,  
867 *Atmospheric Chemistry and Physics*, 23, 6113-6126, 2023a.

868 Zhang, R. and Chan, C. K.: Simultaneous formation of sulfate and nitrate via co-uptake of SO<sub>2</sub> and  
869 NO<sub>2</sub> by aqueous NaCl droplets: combined effect of nitrate photolysis and chlorine chemistry,  
870 *Atmos. Chem. Phys.*, 23, 6113-6126, 10.5194/acp-23-6113-2023, 2023b.

871 Zhang, R. and Chan, C. K.: Enhanced Sulfate Formation through Synergistic Effects of Chlorine  
872 Chemistry and Photosensitization in Atmospheric Particles, *ACS ES&T Air*, 1, 92-102,  
873 10.1021/acsestair.3c00030, 2024.

874 Zhang, R., Gen, M., Huang, D., Li, Y., and Chan, C. K.: Enhanced Sulfate Production by Nitrate  
875 Photolysis in the Presence of Halide Ions in Atmospheric Particles, *Environmental Science &  
876 Technology*, 54, 3831-3839, 10.1021/acs.est.9b06445, 2020a.

877 Zhang, S., Li, D., Ge, S., Wu, C., Xu, X., Liu, X., Li, R., Zhang, F., and Wang, G.: Elucidating the  
878 Mechanism on the Transition-Metal Ion-Synergetic-Catalyzed Oxidation of SO<sub>2</sub> with Implications  
879 for Sulfate Formation in Beijing Haze, *Environmental Science & Technology*, 58, 2912-2921,  
880 10.1021/acs.est.3c08411, 2024.

881 Zhang, S., Li, D., Ge, S., Liu, S., Wu, C., Wang, Y., Chen, Y., Lv, S., Wang, F., Meng, J., and Wang, G.:  
882 Rapid sulfate formation from synergetic oxidation of SO<sub>2</sub> by O<sub>3</sub> and NO<sub>2</sub> under ammonia-rich  
883 conditions: Implications for the explosive growth of atmospheric PM<sub>2.5</sub> during haze events in  
884 China, *Science of The Total Environment*, 772, 144897,  
885 <https://doi.org/10.1016/j.scitotenv.2020.144897>, 2021a.

886 Zhang, T., Dong, J., Zhang, C., Kong, D., Ji, Y., Zhou, Q., and Lu, J.: Photo-transformation of  
887 acetaminophen sensitized by fluoroquinolones in the presence of bromide, *Chemosphere*, 327,  
888 138525, <https://doi.org/10.1016/j.chemosphere.2023.138525>, 2023.

889 Zhang, Y., Wang, K., Tong, H., Huang, R.-J., and Hoffmann, T.: The maximum carbonyl ratio (MCR)  
890 as a new index for the structural classification of secondary organic aerosol components, *Rapid  
891 Communications in Mass Spectrometry*, 35, e9113, <https://doi.org/10.1002/rcm.9113>, 2021b.

892 Zhang, Y., Bao, F., Li, M., Xia, H., Huang, D., Chen, C., and Zhao, J.: Photoinduced Uptake and  
893 Oxidation of SO<sub>2</sub> on Beijing Urban PM<sub>2.5</sub>, *Environmental Science & Technology*, 54, 14868-14876,  
894 10.1021/acs.est.0c01532, 2020b.

895 Zhao, R., Zhang, Q., Xu, X., Wang, W., Zhao, W., Zhang, W., and Zhang, Y.: Effect of photooxidation  
896 on size distribution, light absorption, and molecular compositions of smoke particles from rice  
897 straw combustion, *Environmental Pollution*, 311, 119950,  
898 <https://doi.org/10.1016/j.envpol.2022.119950>, 2022.

899 Zhrebker, A., Rukhovich, G. D., Sarycheva, A., Lechtenfeld, O. J., and Nikolaev, E. N.: Aromaticity  
900 Index with Improved Estimation of Carboxyl Group Contribution for Biogeochemical Studies,  
901 *Environmental Science & Technology*, 56, 2729-2737, 10.1021/acs.est.1c04575, 2022.

902 Zhong, S., Liu, R., Yue, S., Wang, P., Zhang, Q., Ma, C., Deng, J., Qi, Y., Zhu, J., and Liu, C.-Q.:  
903 Peatland Wildfires Enhance Nitrogen-Containing Organic Compounds in Marine Aerosols over  
904 the Western Pacific, *Environmental Science & Technology*, 2024.

905 Zhou, L., Liang, Z., Mabato, B. R. G., Cuevas, R. A. I., Tang, R., Li, M., Cheng, C., and Chan, C. K.:  
906 Sulfate formation via aerosol-phase SO<sub>2</sub> oxidation by model biomass burning photosensitizers:  
907 3,4-dimethoxybenzaldehyde, vanillin and syringaldehyde using single-particle mixing-state  
908 analysis, *Atmos. Chem. Phys.*, 23, 5251-5261, 10.5194/acp-23-5251-2023, 2023.  
909